RESEARCH DEPARTMENT REPORT SERIES no. 32/2007 ISSN 1749-8775

BARFORD ROAD, ST NEOTS, CAMBRIDGESHIRE OPTICALLY STIMULATED LUMINESCENCE DATING OF SINGLE GRAINS OF QUARTZ FROM SEDIMENTARY FILLS OF TWO CURSUS MONUMENTS

SCIENTIFIC DATING REPORT

Ed J Rhodes

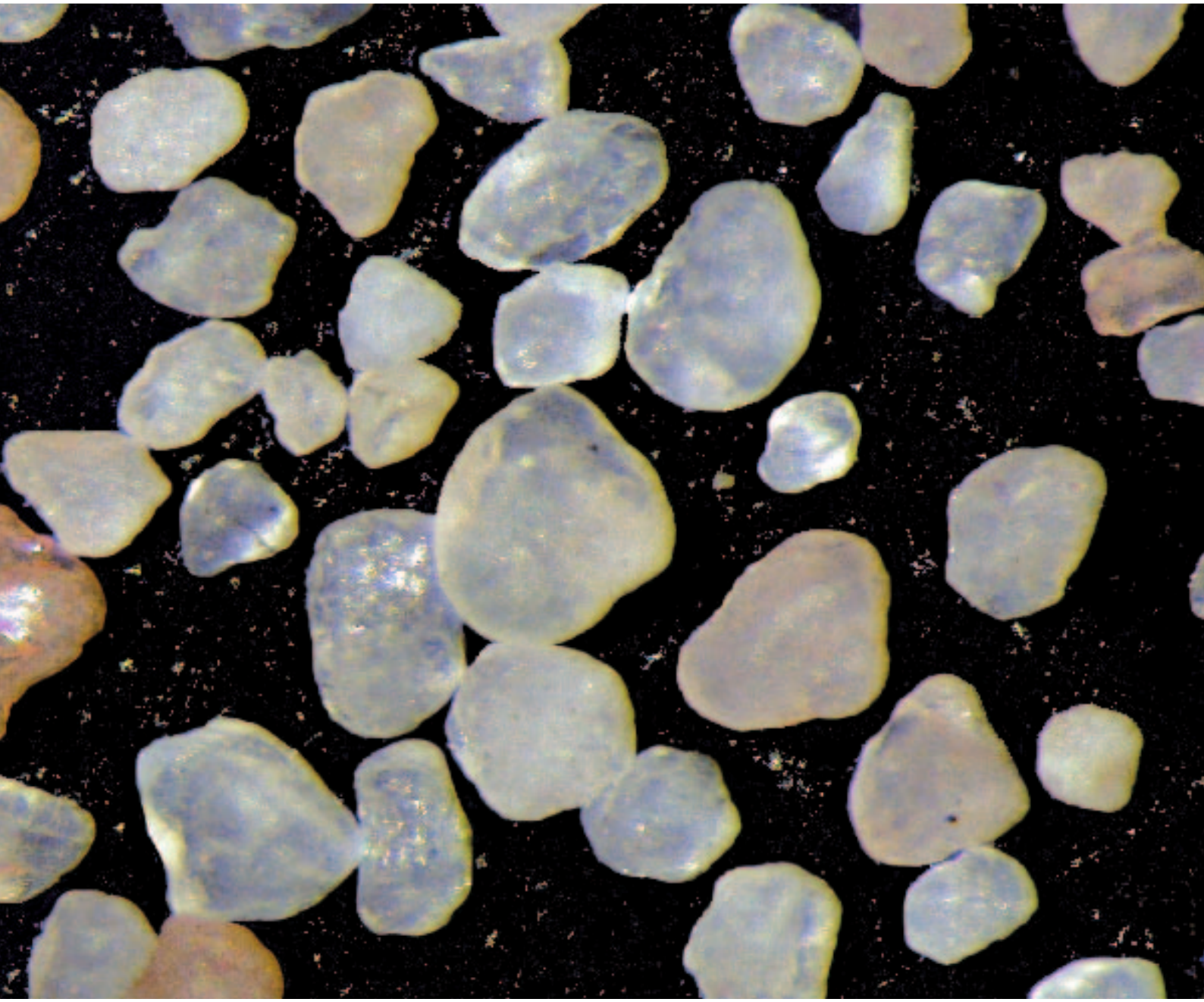

ARCHAEOLOGICAL SCIENCE

ENGLISH HERITAGE

Research Department Report Series 32/2007

Barford Road, St Neots, Cambridgeshire
Optically Stimulated Luminescence Dating of Single Grains of Quartz from Sedimentary Fills of Two Cursus Monuments

Ed J Rhodes

ISSN 1749-8775

Research Department Report Series 32/2007

Barford Road, St Neots, Cambridgeshire
Optically Stimulated Luminescence Dating of Single Grains of Quartz from Sedimentary Fills of Two Cursus Monuments

Ed J Rhodes

Summary

Fifteen sediment samples forming two vertical sequences, one located in the fill of each of two cursus monuments at the site of Barford Road, St Neots, Cambridgeshire were dated using new luminescence methods based on the Optically Stimulated Luminescence (OSL) from single grains of quartz.

From the main suite of results it is concluded that grains showing signs of incomplete zeroing are relatively rare, though more common in basal fill samples. Most samples have a significant grouping of single-grain ages which is likely to represent the depositional age of the sediment. Grains providing significantly younger apparent ages are present in many samples, especially closer to the surface, and probably represent the effects of post-depositional root activity or other bioturbation processes.

A novel approach based on the radiocarbon calibration programme OxCal was developed and applied to provide age estimates for the single grain measurements. The age estimates derived in this manner had relatively high uncertainties, but suggest that the lowermost fill of both cursus monuments began to be deposited in the early to mid 5th millennium BC, and the uppermost samples for both structures were laid down around the 3rd millennium BC.

Keywords

Optically Stimulated Luminescence

Author's Address

Research School of Earth Sciences and Research School of Pacific and Asian Studies, The Australian National University, Canberra, ACT 0200, Australia. Email : Ed.Rhodes@anu.edu.au

Introduction

Luminescence dating has been applied to the dating of ceramics and other heated materials for around 40 years, using the thermoluminescence (TL) signals emitted when mineral grains from a sample are heated in a nitrogen atmosphere. This method was later extended to the dating of sediments, but suffered from the relative insensitivity of the measured signals to natural daylight. This results in high residual signals at the time of deposition, and consequent uncertainties in the age estimates, especially those younger than around 5 to 10 thousand years (Aitken 1985). The introduction of optical dating (Huntley *et al* 1985), based on the optically stimulated luminescence (OSL) signals of quartz measured in the ultraviolet (UV) part of the spectrum while exposing mineral grains to intense green or blue light, overcame many of these problems, and allowed significantly improved reliability in the dating of many sedimentary contexts (Smith *et al* 1990).

Although the multiple aliquot additive dose (MAAD) techniques used for quartz OSL analysis until around the turn of the millennium (AD 2000) appear to provide reliable age estimates for many sedimentary environments, the relatively low precision possible with this technique limited the scope and applicability of the method, particularly for archaeological contexts. Regenerative dose measurements were restricted by severe sensitivity changes observed on heating, following dosing or OSL measurement. These limitations have now been overcome for quartz with the introduction of the single aliquot regenerative dose (SAR) protocol of Murray and Wintle (2000), which incorporates a sensitivity correction determination. This protocol can provide precise equivalent dose estimates over a wide range of doses, and recent assessments of the accuracy of the method are extremely encouraging (Rhodes *et al* 2003). The measurement of several different portions of the same sample can be used to assess internal consistency of equivalent dose values, and therefore identify samples suffering from significant incomplete zeroing.

The SAR protocol can be applied to any single portion of a sample that provides a sufficiently intense luminescence emission for OSL measurement. The technique is therefore ideally suited to determine equivalent dose estimates from single grains of quartz (Bøtter-Jensen *et al* 2000). This approach offers the possibility of making significant enhancements to the reliability of existing luminescence dating methods of sedimentary contexts by providing an assessment of the degree of internal consistency for individual grains. In principle, age agreement of the full population of measured quartz grains can validate conventional OSL techniques or a wide spectrum of apparent ages can indicate the unsuitability of a context for luminescence dating. Further, where more than one discrete population of apparent age is observed, there is the possibility of identifying a reliable subset of fully bleached grains, while rejecting the remaining results from the dating analysis. In the latter case, it may be possible tentatively to identify processes which have affected the sample at or since deposition. The method has been applied to date the earliest Stone Age art in southern Africa (Henshilwood *et al* 2002) in the context of aeolian sand within Blomboss Cave, while Roberts *et al* (1999) were able to demonstrate that previous TL ages for Jinmium Rockshelter, northern Australia represented significant age overestimates. Issues of sample purity and signal zeroing have recently been discussed for Holocene fluvial sediments by Olley *et al* (2003), who demonstrate good agreement between single grain OSL dating and radiocarbon age control.

Research Objectives

This study was undertaken in order to explore the limitations and potential of applying OSL to date contexts where problems of incomplete zeroing might be expected, and to attempt to derive reliable age estimates for the construction and subsequent filling of two cursus

monuments. Single-grain OSL methods were applied, to assess the reliability of conventional multi-grain OSL approaches, and in order to improve the chronological information regarding cursus construction. The original project design incorporated direct comparison of OSL age estimates with radiocarbon age estimates. Samples for radiocarbon dating were collected from the lowermost fill of the cursus monuments, but their dating proved unfeasible as a result of the poor preservation of the organic remains in the rather acid groundwater conditions prevailing at the site (Allen *et al* 2004). This fact emphasises the importance of the development of reliable luminescence dating techniques, which can be applied to sediment fill sequences which are devoid of organic remains.

As a result of the absence of independent age control, the assessment of the OSL methods applied is restricted to determining the internal and stratigraphic coherence and consistency of the data, to observe whether clear patterns are evident from the data, and a more general comparison of the derived age estimates with expected age based on comparison with similar monuments elsewhere.

Sample locations

The archaeological site at Barford Road is located towards the south of St Neots, Cambridgehire (approx location 518000 258500). Fifteen OSL samples were carefully selected so that their results could be compared to form an assessment of the applicability of the single grain approach, based on the stratigraphic consistency and coherence of the dating results. In total, 25 OSL samples were collected from three sections at the site during two visits in early 2001. *In situ* sodium iodide gamma spectrometer measurements to determine the environmental gamma dose rate were made at several locations for each section sampled (15–30 minutes duration each). Sampling was performed by hammering opaque sample tubes of 4cm diameter and either 10 or 15cm length into a cleaned vertical section. OSL measurement was performed on grains isolated from material selected from the central part of each tube, after removal of the sediment at each end under special laboratory lighting conditions. This ensured that no inadvertent light exposure occurred during sampling.

Figure 1 shows the general location of the site beside the Great Ouse, St Neots, Cambridgeshire. Section 1 was located in a complete section across the northern cursus (Fig 2, 5A), dug into gravels of sands, presumed to represent Pleistocene or early Holocene deposits of the Great Ouse. Within this section 14 samples in total were collected, of which 10 were selected for this study (X431, X432, X433, X435, X436, X437, X439, X441, X442, X443). The lowermost samples (X431, X432) represent what was considered by the excavators to be the first sediment deposited in the ditch after construction, while the highest sample (X443) was just 50cm from the surface, under the contemporary soil (Fig 3, 5A). At three levels in Section 1 duplicate samples within the same horizon were measured. The uneven spacing of samples within the section reflects the fact that at certain horizons and locations, stones prevented insertion of the OSL sampling tubes. The sediments were composed

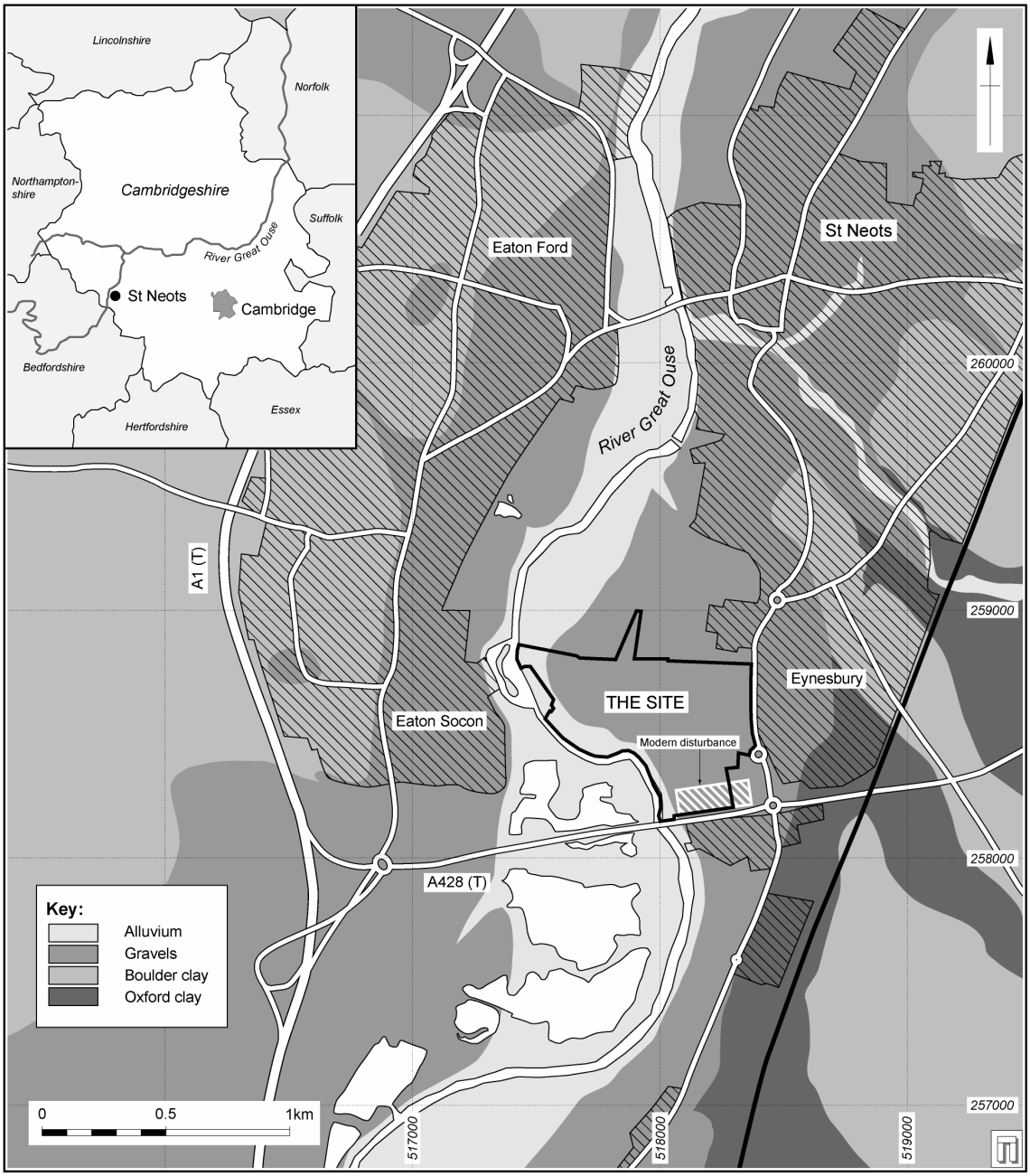

Figure 1: Map showing location and geology of the area of the Site of Barford Road, St Neots (with kind permission of Wessex Archaeology)

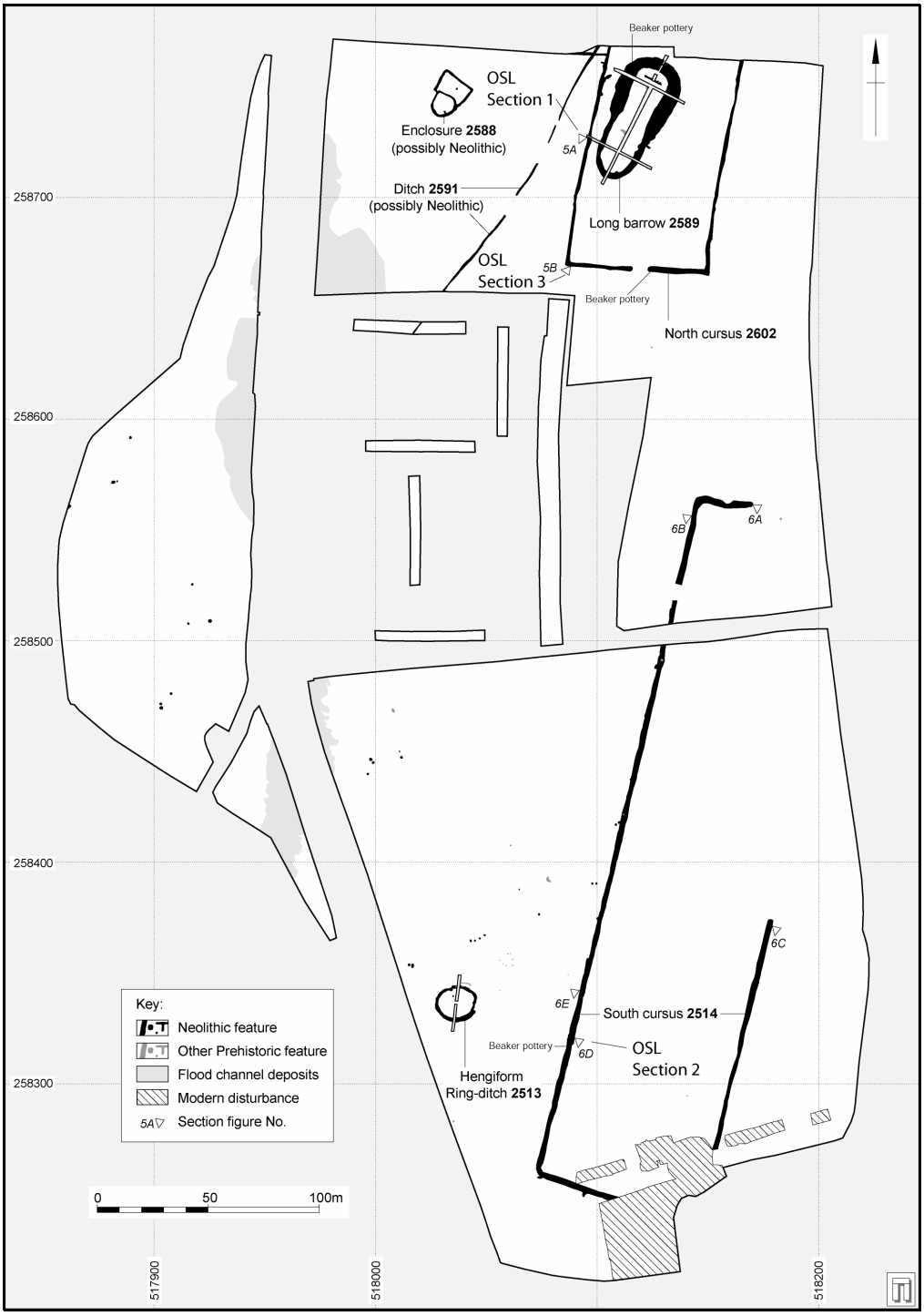

Figure 2: Detailed plan of Neolithic features excavated at the site. The three sections from which OSL samples were collected are termed 5A (Section 1; northern cursus), 5B (Section 3; northern cursus) and 5E (Section 2; southern cursus) (based on a figure provided by kind permission of Wessex Archaeology)

dominantly of silts and fine to medium gravel, with an additional sand fraction. At the time of sampling, approximately vertical structures observed as darker brown to black bands within the brown silty sediments of the section were observed. These had the general appearance of root marks, and the darker colour is thought to represent material introduced from higher in the section.

Section 2 (Fig 2, 6D; Fig 4, 6D) comprised 5 samples forming a single sequence within the fill of the southern cursus (X451 (base), X452, X453, X454, X455). The top 50cm of the section was already removed before sampling commenced, so this was restricted to the lower sediment layers. No sample duplicates were collected, and the much sandier sediment fill, largely devoid of stones, encountered at this section made it difficult to determine the position of the base of the fill. No root marks were observed, though daylight was at very low levels when this section was sampled.

Six samples were collected from a third section (Fig 2, 5B; Fig 3, 5B) in the northern cursus. The sediment fill at this location was largely stone-free and had a higher sand content than did section 1. None of these samples was used for single-grain measurements, though one sample from the base of the section (X445) was measured using conventional multi-grain SAR measurements (Allen *et al* 2004; Rhodes 2002), and those results are reported here. Note that the basal samples were shown as located beneath the primary fill in Allen *et al* (2004), but these appeared to be within fill when collected, and this appears borne out by the OSL age estimate derived. The section in Figure 3 has been modified accordingly. A fuller description of archaeological contexts and sediment characteristics is provided by Allen *et al* (2004).

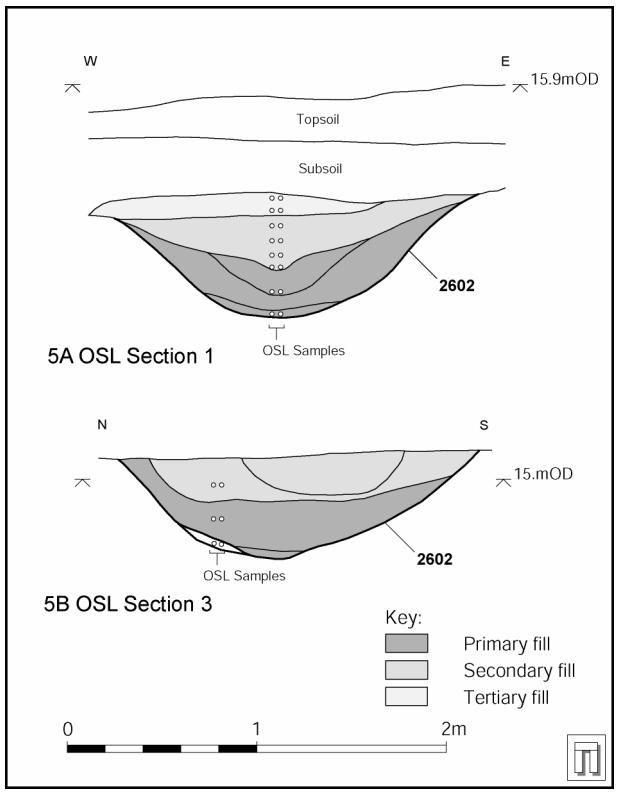

Figure 3: OSL sampling locations, northern cursus. All samples collected are shown, though not all were measured (based on a figure provided by kind permission of Wessex Archaeology)

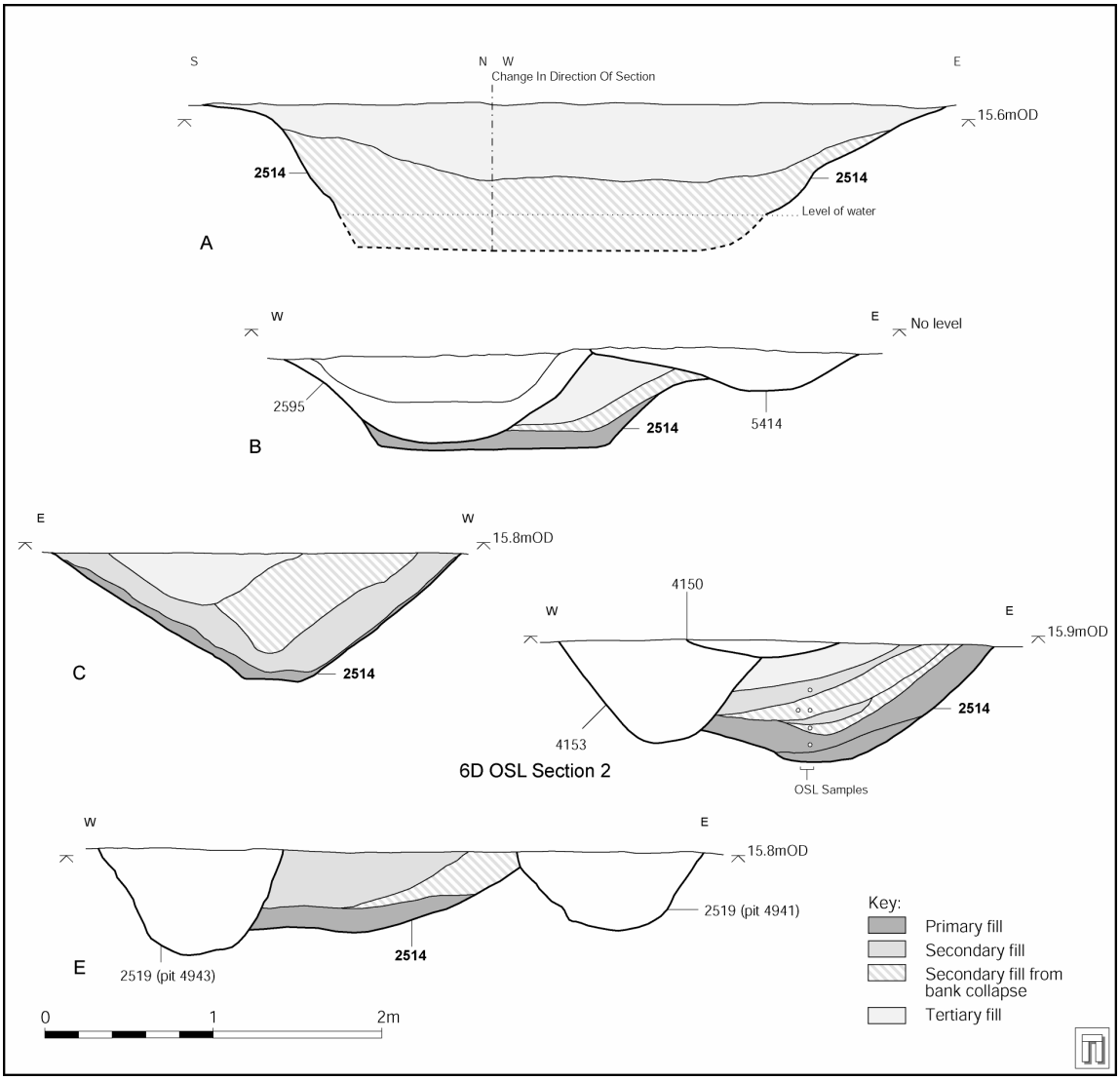

Figure 4: OSL sampling locations and section drawings, southern cursus. See Allen *et al* (2004) for a full description of archaeological contexts and sediment characteristics (based on a figure provided by kind permission of Wessex Archaeology)

Measurements performed

A summary of the different measurements made is provided in Table 1. Measurement conditions are discussed below, and a summary of those used is provided in Table 2.

Multi-grain SAR measurements
To complement the single-grain measurements, conventional multi-grain SAR protocol OSL dates were performed on 8 of the 15 single-grain samples, as well as an additional sample (X445) from the base of a third section located in the northern cursus. Six of these multi-grain SAR measurements had already been made and form the basis of the age estimates for the two cursus monuments at Barford Road, St Neots, described in Allen *et al* (2004), and Rhodes (2001; 2002). Small aliquot SAR protocol measurements were performed on 4 of these 8 samples (X431, X432, X443, X452), as an assessment of this method to detect incomplete zeroing or intrusive grain populations.

Single-grain measurements
For each of the 15 samples forming the basis of this project, 400 single grains were measured. For three samples, additional detailed single-grain measurements were undertaken based on a further 1200 single grains.

An assessment of some of the limitations of single-grain OSL was provided by several further complementary measurements, including a sample blank (empty holder), grains from two pottery sherds previously dated using the conventional SAR protocol, and "dose recovery" tests using the pottery grains and an annealed sample following a range of different treatments. These latter experiments were designed to assess the limitations of precision and accuracy imposed by the Risø luminescence reader and sample analysis procedures, and can be considered as a form of internal reproducibility test.

Table 1 – OSL measurement list

Measurement Group	Type of sample or measurement		Sample code
1	Blank single grain holder run		BLANKAA
2	Recovered dose experiments using single grains		
		Annealed quartz	TVsgaa
		Sensitized quartz (pottery)	X593ab
			X593ac
			X594ab
			X5934ad
3	Pottery single grain measurements		X593sgaa
			X594sgaa
4	St Neots sediment samples, single grain measurements		
	400 grain runs	Section1	X431
			X432
			X433
			X435
			X436
			X437
			X439
			X441
			X442
			X443
		Section 2	X451
			X452
			X453
			X454
			X455
5	St Neots sediment samples, single grain measurements		
	1200 grain runs	Section1	X432
			X443
		Section 2	X452
6	Small aliquot multi-grain measurements, St Neots		
		Section 1	X431
			X432
			X443
		Section 2	X452
7	Standard aliquot multi-grain measurements, St Neots		
		Section 1	X431
			X432
			X443
		Section 2	X451
			X452
			X453
			X454
			X455
		Section 3	X445

Sample preparation

The laboratory procedures described in the present section are designed to yield pure quartz, of a particular grain size range, from natural sediment samples. In order to obtain this material, samples were taken through a standard preparation procedure, as outlined below, based on methods described by Rhodes (1988). All laboratory treatments were performed under low intensity laboratory safe-lighting, from purpose-built filtered sodium lamps (emitting at 588nm).

Each sample was treated with hydrochloric acid (HCl) to remove carbonate. The sample was then sieved to isolate the 125 to 180μm fraction. The selected grain size fraction was then treated in concentrated HF (48%) for 100 minutes. This treatment serves two purposes: (i) to dissolve feldspar grains, and (ii) to remove (etch) the outer surface of quartz grains (the only part of each quartz grain exposed to natural alpha radiation during burial). Heavy minerals present were subsequently removed by centrifuging the sample in a sodium polytungstate solution at 2.68g cm^{-3}. Finally, each sample was re-sieved to remove heavily etched grains. For conventional SAR measurements, the prepared quartz samples were mounted on 1cm diameter aluminium discs using viscous silicone oil. For single-grain measurements, grains were sprinkled onto clean 100-hole single grain discs, and excess grains brushed off using a very fine tipped (size 0000) artist's paint brush. Extreme caution was taken to ensure that all equipment was free of contamination, with extensive repeated cleaning of all tools and surfaces with methylated ethanol, and examination of clean single grain discs with a binocular microscope. Single grains were in all cases mounted immediately prior to measurement.

Various tests for sample purity were made. Quartz does not produce a significant infra-red stimulated luminescence (IRSL) signal at room temperature. Feldspar, the primary source of contamination, does produce luminescence when stimulated with IR at room temperature. The presence of IRSL is therefore used as a criterion for rejection. This is incorporated into the conventional SAR measurements, as a measurement of the natural IRSL signal. In these single-grain measurements, the equipment did not allow the measurement of the IRSL of individual grains. However, a measurement to determine loss of the OSL signal after IR exposure was made (Olley *et al* 2003). Two assessments of the recycling ratio (see Appendix A) were made for each grain, and for the second of these, the regenerative OSL measurement was preceded by an IRSL exposure. Grains whose OSL is sensitive to IR exposure fail to provide an adequate recycling value, and are automatically excluded on the basis of the acceptance/rejection criteria used with the Analyst software. Examination of the IRSL response during several measurement runs shows that a very low proportion of grains were rejected in this manner.

Measurement conditions

Luminescence measurements were made using two automated Risø luminescence measurement readers. For the conventional SAR measurements, optical excitation was provided by filtered blue diodes (emitting ~410–510nm), while for the single grain measurements, excitation was provided by a focussed green (532nm) laser. Luminescence was detected in the ultraviolet region on both systems, using EMI 9635Q bialkali photomultiplier tubes, filtered with Hoya U340 glass filters. Laboratory beta irradiation was provided by sealed ^{90}Sr sources at rates of 1.5–3 Gy/minute depending on the system used.

For the conventional multi-grain SAR measurements D_e values for each sample were obtained for 12 aliquots (see Appendix A for details of calculations). All OSL measurements were made at 125°C (to ensure no re-trapping of charge to the 110°C TL trap during measurement), for 60 seconds in the case of multi-grain measurements, and for 1s for single-

grain measurements. The initial signal with the stable background count rate from the end of each measurement subtracted was normalized (for sensitivity correction) using the OSL signal regenerated by a subsequent beta dose (β_s). To ensure removal of unstable OSL components, removal of dose quenching effects and re-trapping necessary to ensure meaningful comparison between naturally and laboratory irradiated signals, 'preheating' was performed prior to each OSL measurement. A preheat (PH_1) at 220°C for 10s was used following the regenerative dose (β_i), and a preheat (PH_2) of 200°C for 10s was used following each test dose (β_s). See Appendix A for further details of the SAR protocol. These conditions were found to provide good recycling, and provided age estimates with no apparent systematic offset and relatively high precision (around 2%) for archaeological sediments from the Shetland Isles (Rhodes *et al* 2003). Note that using single grains, it is not meaningful to undertake a preheat plateau test. The primary criteria for selecting appropriate preheat conditions is that these treatments provide signals of sufficient thermal stability (Smith *et al* 1986; Rhodes 1988; Rhodes 1990), they minimise thermal transfer (Rhodes 2000), and provide behaviour compatible with SAR measurement (Wintle and Murray 2000; Bailey 2000). The observed recycling ratio (see Appendix A) provides a measure of the latter point; grains falling outside an acceptable range are rejected from the analysis.

The measurement conditions adopted for the single grain measurements are summarized in Table 2, below.

Table 2 – Single-grain measurement parameters

OSL measurement temperature	125°C	Standard
OSL measurement initial pause time	10s	Standard RLAHA
OSL measurement time	1s	Default
OSL measurement power	90% max	Standard RLAHA SG
OSL measurement channel no.	50	Default
Preheat 1 temperature and time	220°C, 10s	Standard RLAHA
Preheat 2 temperature and time	200°C, 10s	Standard RLAHA
Test dose size	3.4Gy	Standard RLAHA SG
No. of dose points	3 + zero + 2	Standard RLAHA SG
IR bleach measurement	Final cycle	Standard
No. of grains	400	Sample dependent
Regenerative dose spacing	Doubling	Standard RLAHA SG
Holder location parameters 1	1st search, 20μm	Standard RLAHA SG 1
Holder location parameters 2	2nd search 2μm	Standard RLAHA SG 2

Some problems were encountered in single grain measurement, and these are described in Appendix D. In Table 2, "Standard" alone means that this is the usual condition used widely within the luminescence dating community, "Standard RLAHA" means that this condition is usual for measurements made within the Luminescence Dating Laboratory at the Research Laboratory for Archaeology and the History of Art (RLAHA), University of Oxford, and "Standard RLAHA SG" means usual conditions for single grains at RLAHA. The holder location parameters are discussed in Appendix D.

Experimental results

Results of several measurement sequences of additional samples (annealed quartz and pottery samples) were important in guiding the selection of measurement and analysis options for the sediment samples. These are presented in an order designed to assist the

reader in understanding the selection of measurement and analysis parameters for the sediment samples.

Blank holder
This measurement comprised the measurement of a complete dating run for a single (100 hole) empty single grain holder following a 6.75 Gy beta dose. This was to test the assumption that the cleaned empty holder would not produce any apparent signals from contamination or measurement artefacts. No response was observed, and this demonstrates the absence of signals in the absence of sample grains.

Annealed quartz samples
Single grains of 125 to 180μm sieved from crushed fragments of a large single crystal of Madagascan vein quartz (Adamiec 2000, sample EJR01) were measured using a full dating sequence, after administration of a dose of 6.75 Gy. The sample had been heated to 1200°C for 20 hours to sensitize it before crushing and sieving. One hundred grains were measured in a single run (TVsgaa). This run was planned in order to assess the limitations of the machine reproducibility, as it would be expected that this sample represents something close to an idealized material, having a single source and high sensitivity. Figure 5a shows the measured range of doses, shown as a probability distribution function. This has a clear peak at around 7 Gy, but also has outlying points, and a standard deviation of 22%.

Some of the grains have very low signal intensity, while some have high sensitivity but show unacceptable behaviour. In order to include only those grains with acceptable behaviour and significant signal magnitudes, acceptance/rejection criteria need to be selected. The acceptance/rejection criteria for single-grain results is a complex issue, and these issues are discussed further below. The acceptance/rejection criteria used in this analysis were 10% for recycling threshold, test dose uncertainty, and D_e uncertainty; 11 grains had results that matched these criteria. A weighted mean value 6.90 Gy compared to a given dose of 6.75 Gy was measured, a difference of 2.2%.

This experiment illustrates several very important points, which are key to the interpretation of the sediment data from Barford Road.

1 The equipment and analysis procedures which form the basis of all the single grain measurements reported here are capable of recovering a mean dose value close to the given dose.

2 High and low D_e values may be observed for individual grains, even when the average behaviour is apparently good. It is not clear what causes this dose dispersion, which may come from several sources including sample and machine-related factors.

Pottery samples
Two sherds of Neolithic pottery from the Ivory Coast, Africa were measured using single grains. These samples are useful, as they represent groups of grains with homogeneous signal resetting (at the time of firing) but natural dosing conditions. Measurements of the dose received during burial are shown in Figs 5b and 5c for samples X593 and X594 respectively. 400 grains were measured for each, and using acceptance/rejection criteria of 10% for recycling threshold, 15% for the test dose uncertainty, and 25% for the D_e uncertainty, these samples had many grains with significant results; 202 grains for sample X593 and 133 for X594 had results that matched these criteria.

Both show a single peak and again surprisingly wide dispersion in D_e values, with sample X593 having a standard deviation of 29% and X594 17%. Restricting the acceptance/rejection

criteria for sample X593 to 5% for the recycling threshold, test dose uncertainty, and D_e uncertainty reduces the standard deviation to 17% (from 29%), but reduces the number of grains contributing to 20 (from 202). These results illustrate further important points.

3 Restricting the acceptance/rejection criteria for observed single-grain behaviour tends to decrease the observed dispersion, but reduces the number of results significantly.

4 Naturally dosed samples with homogeneous OSL signal resetting provide single grain D_e populations with significant dispersion between values.

Some of the variations in single-grain values for naturally dosed samples may arise from variations in natural beta dose rates in the burial environment. This effect has been modelled using Monte Carlo methods by Nathan *et al* (2003), though for most environments is not likely to exceed 10 to 15%. This is consistent with single-grain observations made for pottery from Swaziland, where standard deviations of D_e populations varied from 10 to 15%.

The same pottery samples were subsequently used to make dose recovery tests, again primarily to assess the D_e population dispersion observed under optimal conditions for bright samples. Similar sized standard deviations were observed for each of these measurements; these were in no case better than around ±10 to 12%. Figures 6a and 6b are examples which illustrate this series of measurements.

The following conclusion is drawn from all of the above experiments using grains from non-sedimentary sources.

5 Technical or intrinsic factors currently limit the measurement of meaningful single grain D_e values with a precision better than around ±10%.

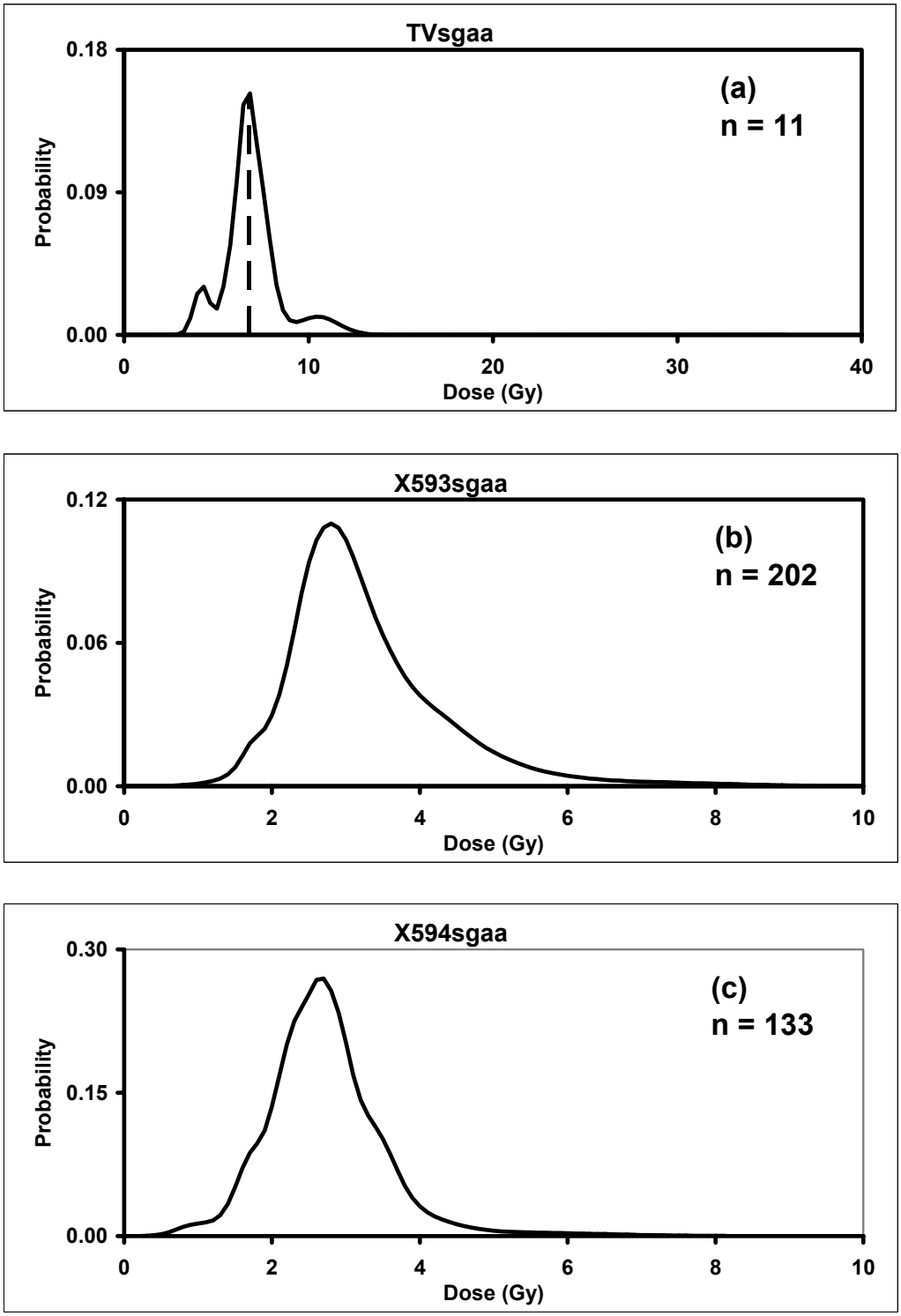

Figure 5: Dose distributions for single grains from heated samples. Plot (a) is the distribution measured for grains of an annealed, crushed, and sieved sample of Madagascan vein quartz (Adamiec 2000 sample EJR01) following a 6.75 Gy laboratory beta dose, based on 11 significant grains from 100 measured. Plot (b) is the single grain OSL dose distribution from a sherd of Neolithic pottery (X593) from the Ivory Coast, West Africa, based on 202 grains from 400 measured. Plot (c) is the single grain OSL dose distribution from a sherd of Neolithic pottery (X594) from the Ivory Coast, West Africa, based on 133 grains from 400 measured. See text for further details

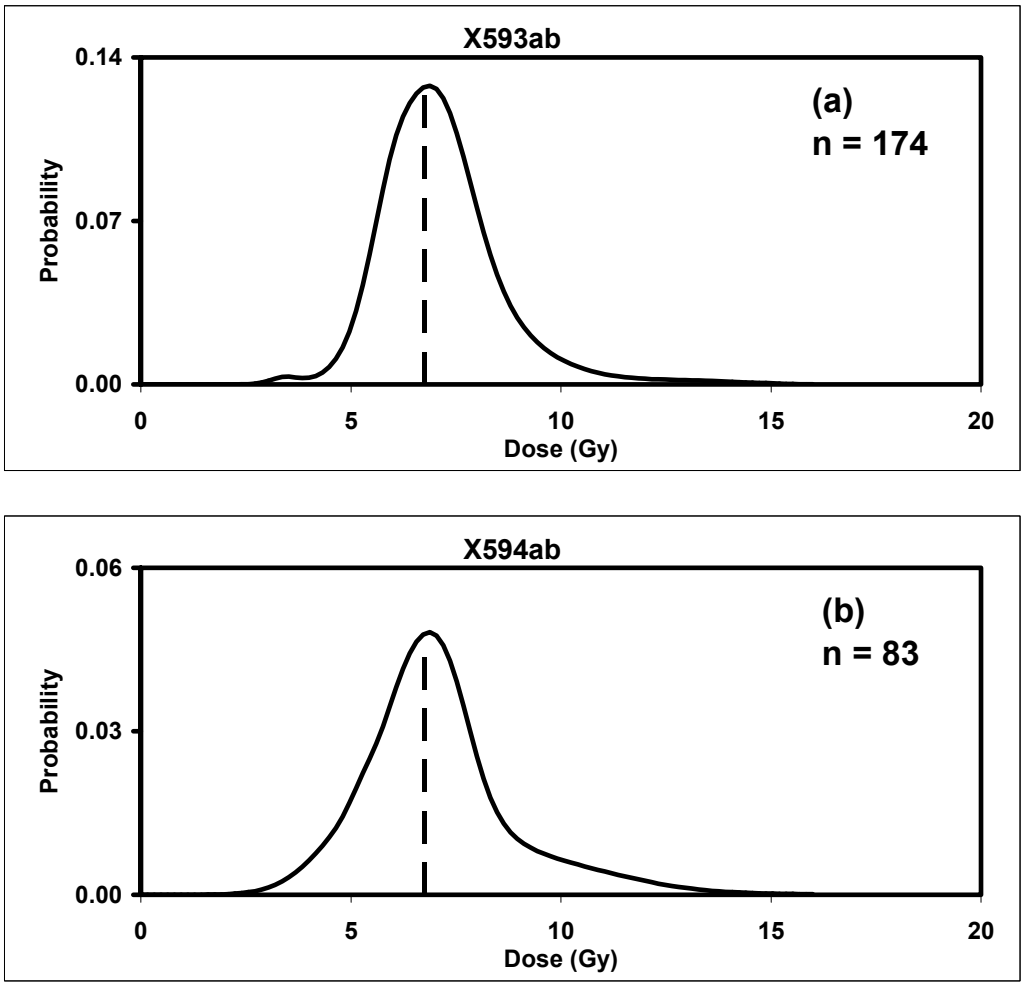

Figure 6: Dose distributions for single grains from heated samples. Plot (a) is the distribution measured for grains from a sherd of Neolithic pottery (X593) from the Ivory Coast, West Africa, following a 6.75 Gy laboratory beta dose, based on 174 grains from 400 measured. Plot (b) is the distribution measured for grains from a sherd of Neolithic pottery (X594) from the Ivory Coast, West Africa, following a 6.75 Gy laboratory beta dose, based on 83 grains from 400 measured. See text for further details

Summary

The above measurements with results shown in Figures 5 and 6 clearly demonstrate that, while mean values of dose can be recovered using single grains, there are effects present which cause significant dispersal of D_e results. This leads the present author to the conclusion that including a higher number of grains with slightly less significance and precision to each measurement is probably the best strategy for determining single grain ages from real sedimentary samples. Some of these issues are dealt with in greater detail by Truscott *et al* (2000).

Acceptance/rejection criteria of single grain measurements

This is perhaps the most difficult aspect of single-grain measurements at present. There are two distinct stages to the arrival of a single-grain age estimate. Stage 1 is the selection of criteria for including measured D_e determinations in the sample D_e distribution. Stage 2 is the selection of a (possibly complete) subset of this distribution to represent the best D_e estimate for this sample, and consequently the optimal age estimation.

As rejection criteria are stiffened, ie inclusion is restricted only to those grains displaying only "optimal characteristics", fewer and fewer grains are included in the sample D_e distribution. As the number of included grains decreases, the significance of the resulting distribution is inevitably reduced. The number of grains observed which have "optimal characteristics" depends on a) the characteristics of all grains in the dating sample, and b) the number of grains measured. While the second parameter, the number of grains measured, may be changed within limits imposed by machine-time constraints (but for most samples *not* limited by preparation volume considerations), the first parameter, the characteristics of the grains sampled from the archaeological or geological context is not within the operator's control. There is a balance to be struck between measuring larger numbers of grains more superficially, or measuring a smaller number of grains with a greater precision for each measurement.

Similarly, in the analysis, the operator may select larger numbers of grains, including those with sub-optimal characteristics (such as poorer recycling, lower OSL sensitivity, or more irregular growth characteristics) by selecting relatively wide inclusion criteria. Alternatively, using the same dataset, the operator can select much more restrictive inclusion criteria, and include a smaller subset of the grains, restricted to those with the best characteristics, as assessed from the dataset. As there are three principal parameters that may be used as rejection/inclusion criteria, namely recycling threshold, test dose uncertainty and equivalent dose uncertainty (listed in Table 3 as "analysis dependent"), the selection of the most appropriate combination is essentially a 3-dimensional minimization problem. As there are several other parameters that may be changed in the analysis stage such as the initial and background window lengths and positions (also listed as "analysis dependent" in Table 3), this provides a complex problem.

The approach adopted here has been to make a prior decision about the magnitude of these three principal selection parameters (at 10% recycling, 15% test dose uncertainty, and 25% D_e uncertainty respectively), and analyse all the single-grain measurements using these. The selection was set so that it was likely that grains would be included for all samples measured (based on experience of other UK sediment samples). Had the samples come from a different location (such as Australian fluvial sediments or UK hearth contexts, both of which include a higher concentration of sensitive grains), these could have been set more restrictively, but it is felt that this combination represents a pragmatic compromise between precision and significance.

Table 3 – Single grain analysis parameters

Growth curve fitting programme	Analyst	Standard RLAHA SG
Growth curve	Exponential + Linear	Sample dependent
Include / exclude recycled points	Exclude	Analysis dependent
Initial OSL window, time	0.10s	Analysis dependent
OSL background window, time	0.22s	Analysis dependent
Acceptance/rejection criteria for D_e distribution		
Signal > 3 sigma above background	Yes	Standard
Recycling threshold	10%	Analysis dependent
Test dose uncertainty	15% see Appendix D	Analysis dependent
Equivalent dose uncertainty	25%	Analysis dependent
Reject mis-fitted grains	Yes	Standard RLAHA
Reject remaining negative values	Yes	Analysis dependent
Restore De uncertainty when zero	Yes	Analysis dependent

Condition descriptions are as for Table 2. See Appendix D for more complete description of terminology used.

Single-grain results for Barford Road samples

Using the measurement conditions described above, single-grain measurements have been made for quartz grains from 15 sediment samples representing the ditch-fill deposits of two cursus monuments from this site. Using the acceptance/rejection criteria described above these have been analysed and are displayed in Figures 7 and 8. These distributions have been converted from D_e populations to age estimate distributions by dividing each D_e value by the mean dose rate for that sample. These were determined by *in situ* gamma spectrometry for the gamma dose rate, neutron activation analysis (NAA) determination of U, Th, and K content was used to calculate the beta dose rate using the conversion factors of Adamiec and Aitken (1998) and the attenuation factors of Mejdahl (1979). Cosmic dose rate contributions were calculated using the formulae of Prescott and Hutton (1994), and the water attenuation was estimated using the formulae given by Aitken (1985). As mentioned above, the mean dose rate does not necessarily apply equally to every grain, and this effect may be responsible for some of the observed dispersion of naturally dosed grains, but use of the mean value should provide age estimates without systematic bias.

Figure 7 shows the age distributions for the quartz single grain OSL results for the 10 samples from Section 1 in the northern cusus, plotted as probability versus age before 2000 AD. These (and all further probability distribution function (pdf) plots shown) are the normalized sums of the individual Gaussian age distributions for each grain measured for that sample, with an additional 5% uncertainty added in quadrature to eliminate the misleading effects caused by values with apparent high precision. 5% is considered a reasonable value, which allows the structure of the different measurements to be observed, while reducing the influence of the most precise individual values. The sample codes and their respective numbers of grains included in each distribution are shown, and the plots are arranged on the page in approximate stratigraphic position. The three repeat sample pairs measured can be seen clearly, with samples X431 and X432 at the base of the sequence, and sample X443 being the highest sample collected at that location. As is the case for the pottery and annealed samples, the distributions are relatively wide. Some appear uni-modal (such as X437) while others have multiple distinct peaks (eg X435, X439, X443). The samples clearly demonstrate a degree of internal consistency, with most having a dominant peak at around 7,000 to 4,000 years before present. Only two samples have peaks higher than this (X431 and X432 both from the base having 1 and 2 higher peaks respectively), while others show signs of higher shoulders (X433, X436, X439, X442), though these tend to be small in comparison to lower peaks. Four of the samples (X435, X439, X441, and X443) show well-defined lower peaks. The stratigraphic incoherence of these age distribution contributions, specifically their absence in samples X437 and X442 strongly suggest that this represents the effects of younger grains introduced into the samples. The fact that these values are not zero strongly suggests that these do not represent laboratory contamination (where cleaning of equipment occurs in daylight and OSL signal resetting of any residual grains should be expected). The field observation of the presence of dark

vertical or sub-vertical structures within the sediment, interpreted as root casts or similar bioturbation indicators is consistent with this conclusion.

Figure 8 shows similar plots for the quartz single-grain OSL results for the 5 samples from section 2, in the southern cursus. A similar pattern is observed for these samples. Only the basal sample (X451) shows signs of clear peaks above the main grouping, while 4 samples show signs of younger grains. Sample X452 demonstrates a very well-defined single peak.

It is not clear or obvious how to proceed from these distribution to calculate an optimal age estimate for each sample, and certainly not obvious how to estimate the uncertainties in any value or range produced. Rigorous testing of the procedures adopted in conventional multi-grain SAR OSL by comparison to ^{14}C AMS dating by Rhodes *et al* (2003) for archaeological sediments appears to confirm their validity. For those samples, the D_e estimate used represented the weighted mean of the 12 measured aliquots divided by root n (n = 12) to give a standard error estimate of the value. Testing using the internal consistency of Bayesian methods suggested that no significant systematic error was present, and that the precision-only uncertainties of all of the components required for age estimation (including those on the D_e results estimated as described above) approached a reasonable representative assessment of the variability between samples, at levels of ±1.5 to 3%.

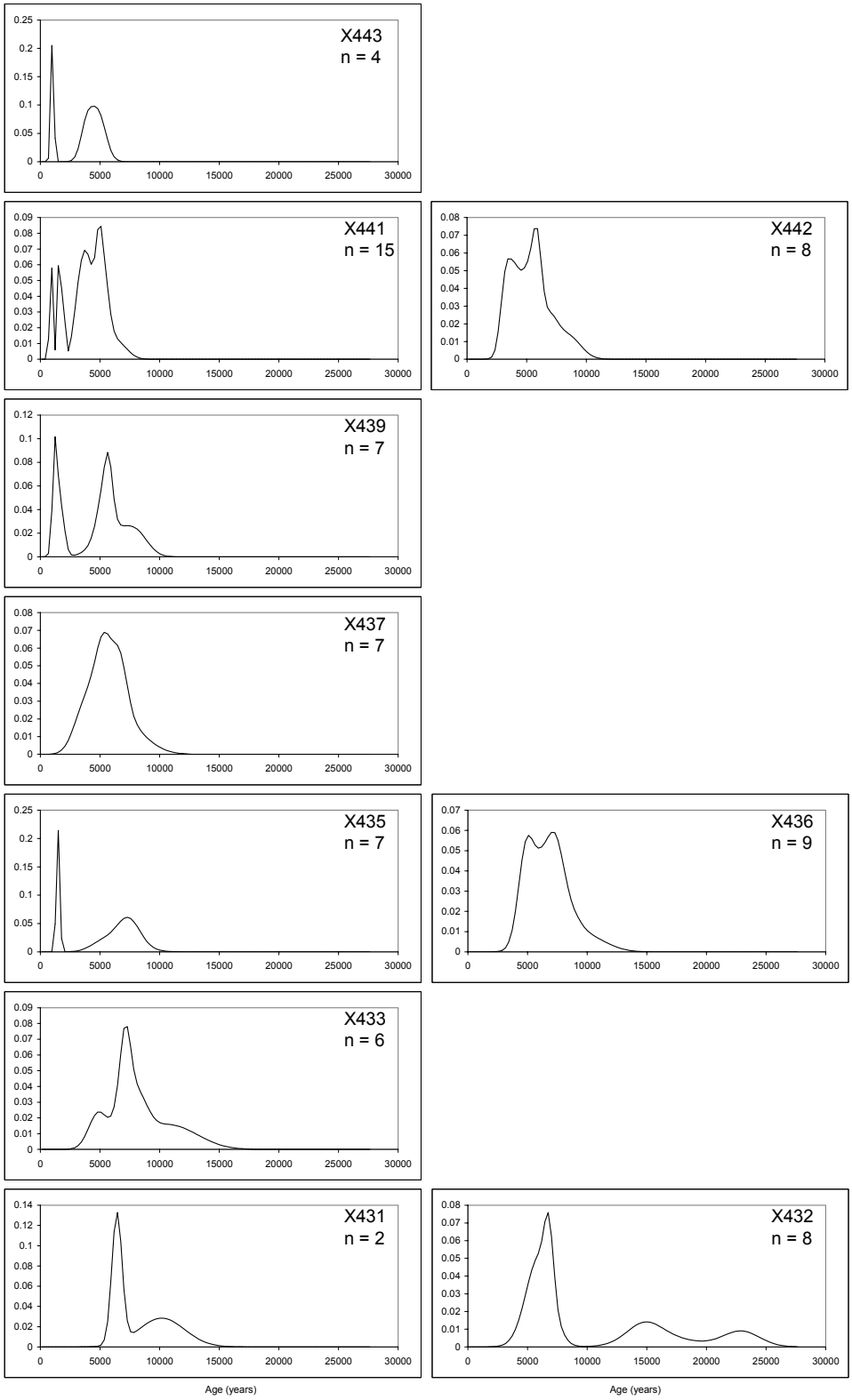

Figure 7: Single-grain age distributions for the 10 samples from Section 1, northern cursus, Barford Road, St Neots. Plots are probability distributions versus age in years before 2000 AD, and the locations of the plots are in approximate stratigraphic position for ease of comparison (sample X443 at the top, samples X431 and X432 at the base). Sample codes and the numbers of grains contributing to each plot are provided. See text for further details

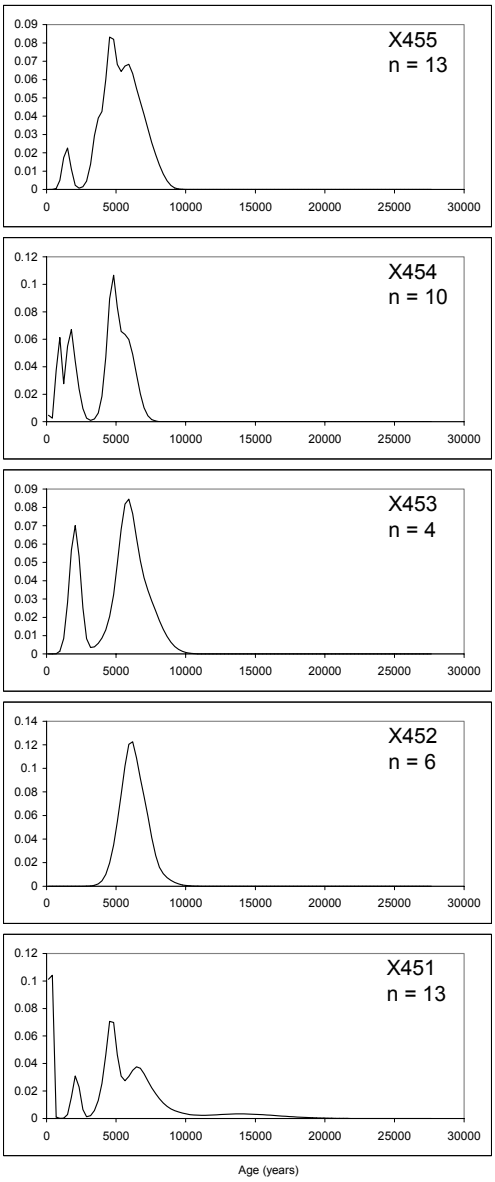

Figure 8: Single-grain age distributions for the 5 samples from Section 2, southern cursus, Barford Road, St Neots. Plots are probability distributions versus age in years before 2000 AD, and the locations of the plots are in approximate stratigraphic position for ease of comparison (sample X455 at the top, sample X451 at the base). Sample codes and the numbers of grains contributing to each plot are provided. See text for further details

However, the primary purpose in making single grain measurements is to detect incomplete zeroing or grain mixing effects, and omit sub-samples suffering from these effects. Therefore, there exists a significant philosophical problem of which single grain results to include and which to omit. With the application of a specific model such as that which expects occasional higher values related to grains with poorly reset OSL signals, or the incorporation of younger values by root activity, strongly deviant single results such as the 2 highest values for sample X432, or the lowermost value for sample X453 could be omitted. However, it seems unjustifiable to the present author to take a standard error estimate of the remainder, when the inclusion of grains showing subtle over- or under-estimates of D_e might remain. Experience of samples from well-dated contexts and the application of more subtle statistical methods may well shed light on these issues in the future. At present, the use of the raw age distributions as input (prior distributions) within OxCal, and making use

of the stratigraphic information relating the samples appears to represent a pragmatic and reasonable means to proceed, while making as few assumptions as possible. The results of this procedure are provided below.

Comparison of single grain and multi-grain results

Standard multi-grain aliquots (representing approximately 1000 grains) were made for 8 of the samples (plus an additional sample from the base of section 3, X445), while small-aliquots of approximately 150 grains were made for 3 samples (X432, X443, and X452). For sample X431 a set of smaller multi-grain aliquots with around 75 grains each was made. The number of "bright grains", and the nature of the natural grain sensitivity distribution control the degree to which the results from small multi-grain aliquots may approach those from single grains. An important controlling factor is the magnitude, and the presence of any systematic variation within, the signal from the dimmer grains, which may still contribute more counts than that of the few bright grains.

The results from sample X431 are shown in Figure 9. The top distribution shows the results from the two grains (from 400 measured) included in the single grain D_e distributions, while the middle graph shows the results from 12 small aliquots, and lowermost graph, those from 12 standard aliquots. There is a very striking contrast between the results of standard aliquots and small aliquots. The large apparent peak at around 15Gy in the standard aliquots is presumably an artefact of central limit theorem, in which comparing means sampled from a wide distribution provides apparent consistency, and hides the original form of the D_e distribution. With only 2 single grain results, it is difficult to comment on these (though both are consistent with the overall age estimate for the sample), while the very low intensity of most of the small aliquot results renders this distribution very difficult to interpret.

The following samples (X432, X443, and X452) were selected for more detailed study as they demonstrated interesting single grain distributions. Sample X432 showed evidence of poorly reset grains in the age distribution based on 400 single grains (Fig 7, bottom right). Figure 10, upper plot shows the single grain D_e distribution from the measurement of 1600 single grains (including the 400 in Fig 7). Twenty-nine results were included. The same main features of the distribution are retained, suggesting that they are meaningful, and an additional low value at around 1.5 Gy is observed. The 12 small aliquot measurements in the central plot show broadly the same features, though with possibly a little bias to a higher value for the highest peak. The standard aliquot values show a wide range of values, and the most significant dose from the single grain measurements is hardly represented.

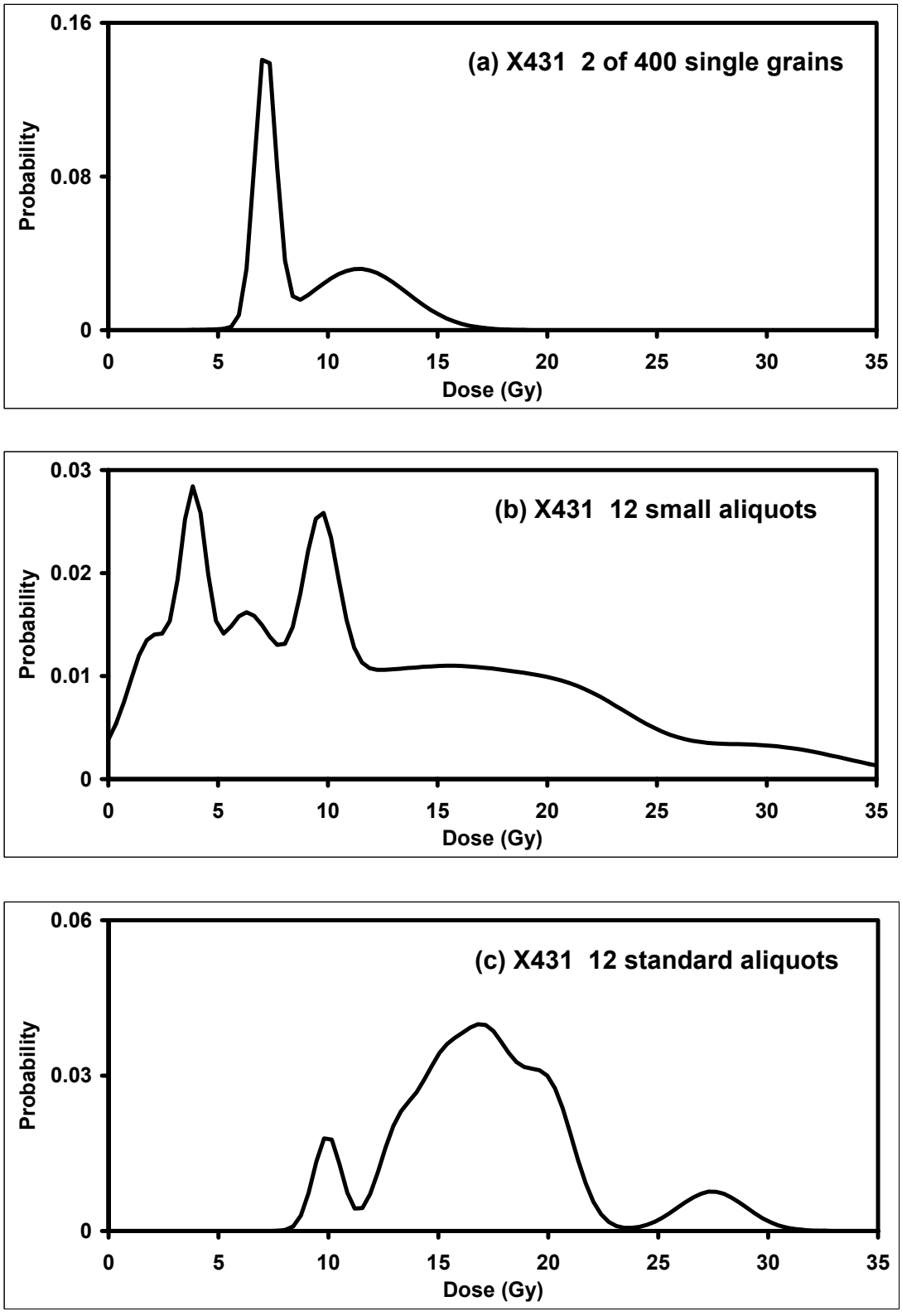

Figure 9: Natural dose distributions for sample X431, based on (a) 2 grains with significant results from 400 measured, (b) 12 small aliquots (approximately 75 grains per aliquot), (c) 12 standard aliquots (approximately 1,000 grains per aliquot). Note the significantly higher dose value for the large peak for the standard aliquots

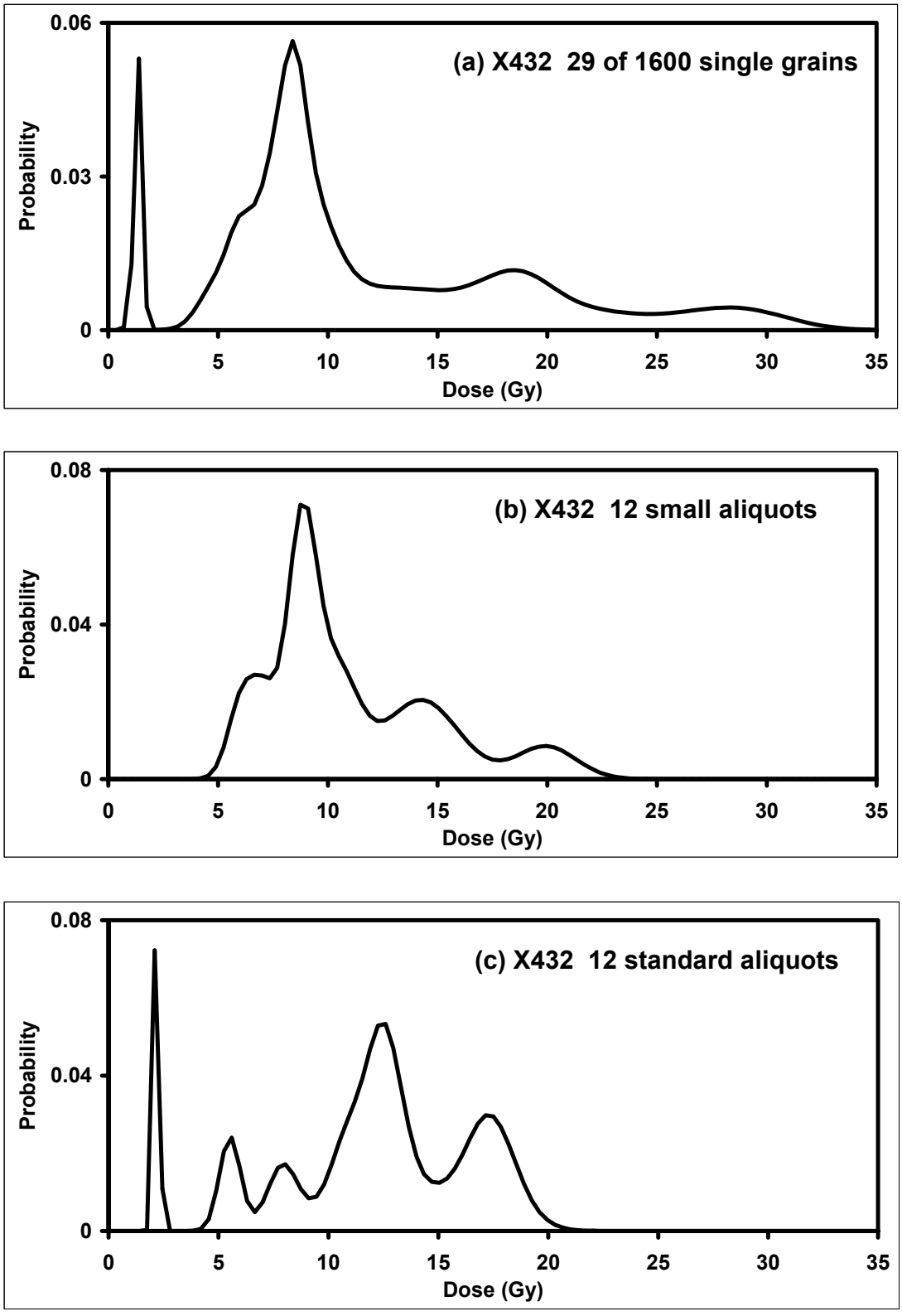

Figure 10: Natural dose distributions for sample X432, based on (a) 29 grains with significant results from 1600 measured, (b) 12 small aliquots (approximately 150 grains per aliquot), (c) 12 standard aliquots (approximately 1,000 grains per aliquot)

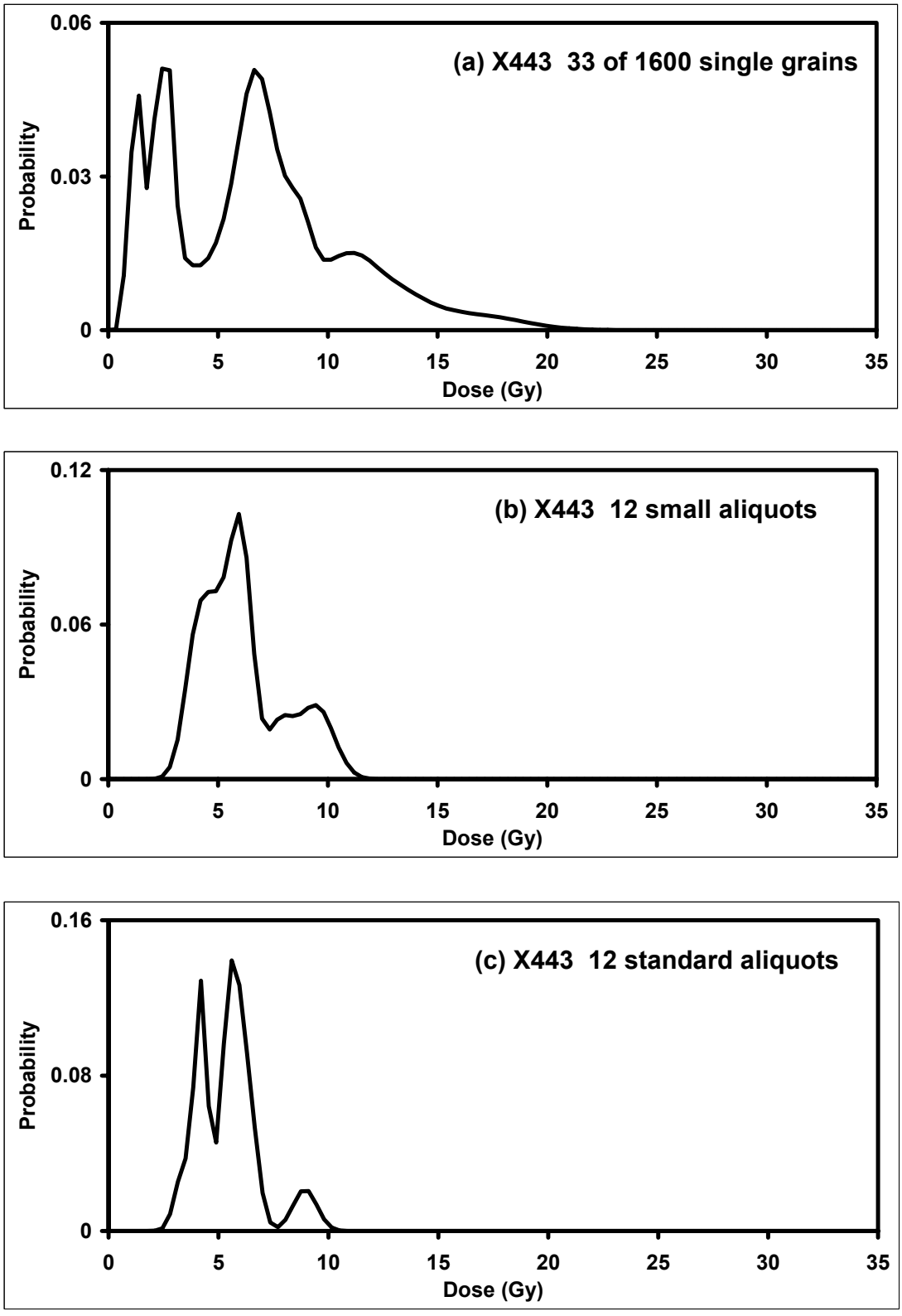

Figure 11: Natural dose distributions for sample X443, based on (a) 33 grains with significant results from 1600 measured, (b) 12 small aliquots (approximately 150 grains per aliquot), (c) 12 standard aliquots (approximately 1,000 grains per aliquot)

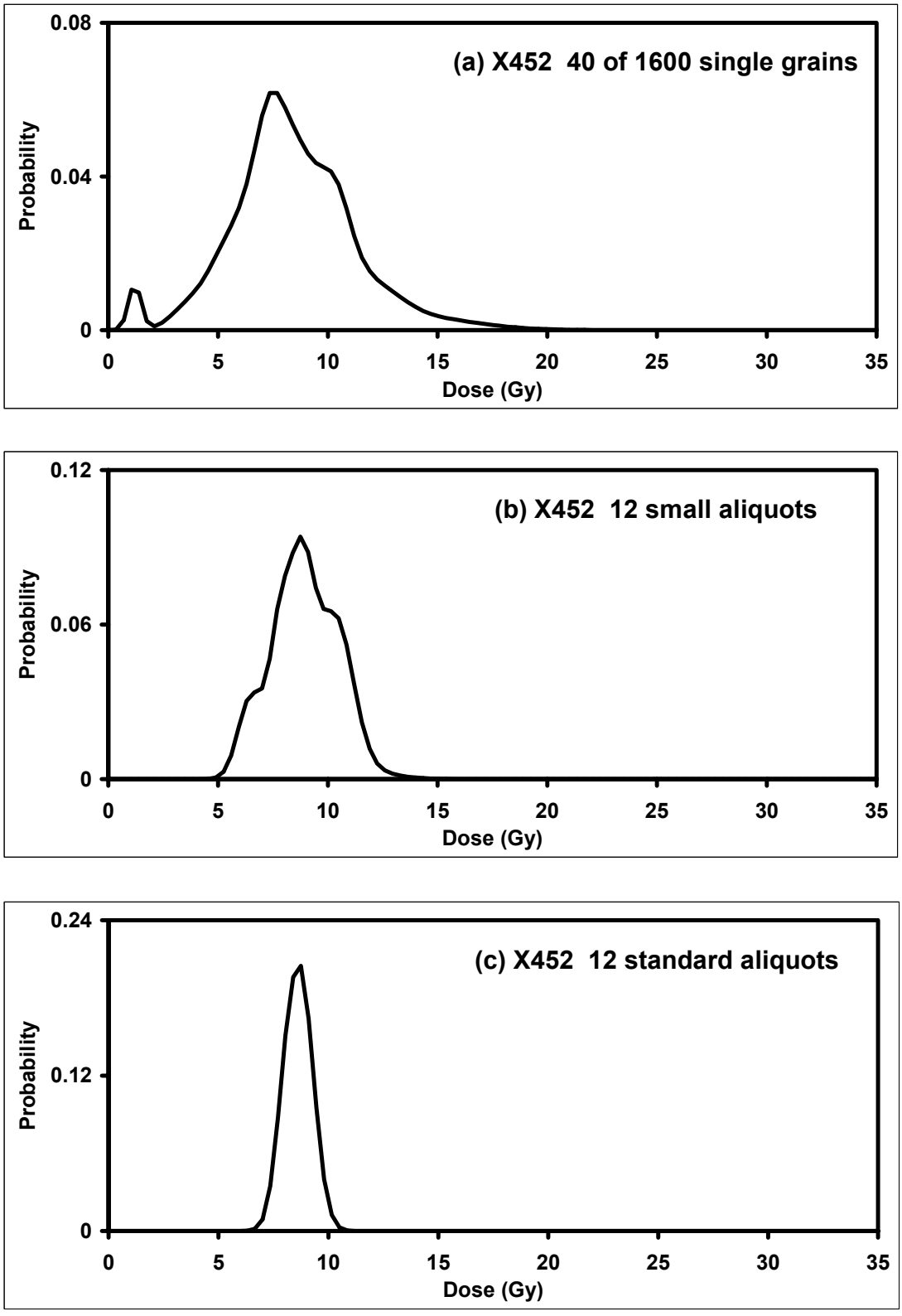

Figure 12: Natural dose distributions for sample X452, based on (a) 40 grains with significant results from 1600 measured, (b) 12 small aliquots (approximately 150 grains per aliquot), (c) 12 standard aliquots (approximately 1,000 grains per aliquot)

Sample X443, shown in Figure 11 again shows departure from the single grain distributions for the small and standard aliquots, which mimic each other, and appear to lose the lower (presumed intrusive) D_e values. The 1600 grain (33 results) distribution has broadly the same features as those based on 400 grains (4 results). Sample X452 showed a single peak in the distribution based on 400 grains (Fig 8). This is similar to the standard aliquot D_e distribution, while the more detailed single grain measurements based on 1600 grains (40 results) and the small aliquot distribution both show more broadening (Fig 12). Both the standard and small aliquot distributions appear to show some subtle bias to higher dose values, presumably from dimmer, and possibly more poorly reset, grains.

The values based on 12 standard aliquots from the remaining 5 samples are not shown as distributions, but their D_e values are given in Appendix B.

Summary
Standard aliquots may give misleading results in comparison to single grain measurements, as would be expected when D_e distributions contain higher or lower values. Small aliquots may approach some of the detail of single grain measurements, but may erode some significant features, and it is possible that they may suffer from bias in dose value from the light sum of the dimmer grains. Single grain measurements based on 400 grains appear to identify many of the features observed using 1600 grains, though the low number of grains with suitable signal size and characteristics means that 400 grains is probably well below an optimal measurement number for samples from similar contexts to those measured in this study.

Table 4 – Age estimates based on standard multi-grain aliquots

Sample	Depth (cm)	Aliquot no. incl/meas	Age years AD/BC	1 sigma uncertainty
Northern cursus, Section 1				
X443	53	11/12	1310	± 350 BC
X431	115	6/12	14,100	± 990 BC
X432	115	10/12	7430	± 630 BC
Northern cursus, Section 3				
X445	100	12/12	4420	± 350 BC
Southern cursus, Section 2				
X455	81	12/12	2690	± 260 BC
X454	88	12/12	2990	± 310 BC
X453	90	10/12	3280	± 250 BC
X452	100	12/12	4100	± 300 BC
X451	110	11/12	4400	± 350 BC

Age estimation

The age estimates based on 12 standard multi-grain measurements are given in Table 4 for the 9 samples measured in this manner, listed in stratigraphic order.

The age estimates from Section 2 and Section 3 appear reasonable on archaeological grounds, as representing the earliest Neolithic (Allen *et al* 2004). While the age estimate for sample X443 may be sensible, those for the basal samples X431 and X432 from Section 1 appear too old on archaeological grounds. The comparisons with single grains shown in Figures 9 and 10 appear to bear this out, and suggest that these measurements contain significant contributions from poorly reset grains.

Table 5 – Age estimates based on small multi-grain aliquots

Sample	Depth (cm)	Aliquot no. incl/meas	Age years AD/BC	1 sigma uncertainty
Northern cursus, Section 1				
X443	53	9/12	1680	± 280 BC
X431	115	8/12	3890	± 1930 BC
X432	115	8/12	4430	± 710 BC
Southern cursus, Section 2				
X452	100	12/12	3640	± 370 BC

The age estimate results from the small aliquots (Table 5) all appear consistent with the archaeological expectations (Allen *et al* 2004), but differences between some of these and the single grain measurements are discussed above, and shown in Figures 9–12. For all the results in Tables 4 and 5, a subjective judgement was made as to which of the 12 measured aliquots to include in the analysis, and which to omit. These tables show the number of aliquots included in the calculation of the age estimate presented besides the number measured which is 12 in each case. While more rigorous criteria could be established for inclusion or rejection of results from individual aliquots, this will vary with OSL characteristics and between samples, and remains a problem.

Single-grain age estimates

As mentioned above, there are some problems in converting single grain age distributions into optimal age estimates. Different approaches have been applied by different researchers, with Roberts *et al* (1998) including all results, or selecting lower values, while Roberts *et al* (1999) used central age and minimum age models. The single-grain age distributions determined for the samples from Barford Road, St Neots, derived using the mean dose rates (Appendix C) are shown in Figures 7 and 8. The stratigraphic relationships of the samples, preserved within these Figures, provide some indication of which of the outlying results may represent the age of the sample, or may represent poorly reset grains, or those introduced after deposition by mixing effects. This approach, making inclusion and exclusion judgements on additional stratigraphic data, is the basis of the Bayesian analysis of sample sequences. Many of the issues of applying these statistical methods to luminescence data are discussed at length by Rhodes *et al* (2003). However, some of the more detailed aspects of the approach adopted in that paper (such as the removal and recombination of systematic error contributions, and estimation of USS or "unshared systematic error" values) are applicable to samples with normally distributed errors, but cannot be applied directly to complex single grain distributions.

The data determined for these samples show variations between different single grains significantly greater than the size of systematic errors introduced by calibration uncertainties or likely dose rate estimation errors (Rhodes *et al* 2003). Therefore, a pragmatic approach has been adopted here, in which the age distributions shown in Figures 7 and 8 are used as the priors for an OxCal analysis, and the subsequent output is assumed to have a sufficiently wide range to incorporate all systematic errors. The high agreement indices (Bronk Ramsey 1995) achieved for both sequences (Sections 1 and 2, Figs 7 and 8) suggest that this is probably the case. Certainly, the age estimates derived have significantly wider uncertainties

than those determined on the basis of the standard multi-grain aliquots for Sections 2 and 3 (Table 4).

Figure 13a shows the prior data for Section 1 from the northern cursus, while Figure 13b shows the prior and posterior distributions. These data were analysed using a resolution of 100 years, using OxCal 3.4, and with constructive advice from the program's author. With no need to remove the results from single grains considered to be intrusive or poorly reset, the analysis has determined the most likely age for each sample (posterior distributions), shown in Figure 13b in solid.

Table 6 – Age estimates based on Bayesian analysis of single grain data

Sample	Depth (cm)	Age years AD/BC	1 sigma uncertainty
Northern cursus, Section 1			
X443	53	2500	± 700 BC
X442	60	3100	± 600 BC
X441	60	3100	± 600 BC
X439	67	3500	± 500 BC
X437	75	3650	± 550 BC
X436	85	4050	± 550 BC
X435	85	4100	± 600 BC
X433	99	4500	± 600 BC
X431	115	4800	± 600 BC
X432	115	4850	± 550 BC
Southern cursus, Section 2			
X455	81	2900	± 800 BC
X454	88	3300	± 700 BC
X453	90	3750	± 650 BC
X452	100	4150	± 650 BC
X455	110	4550	± 850 BC

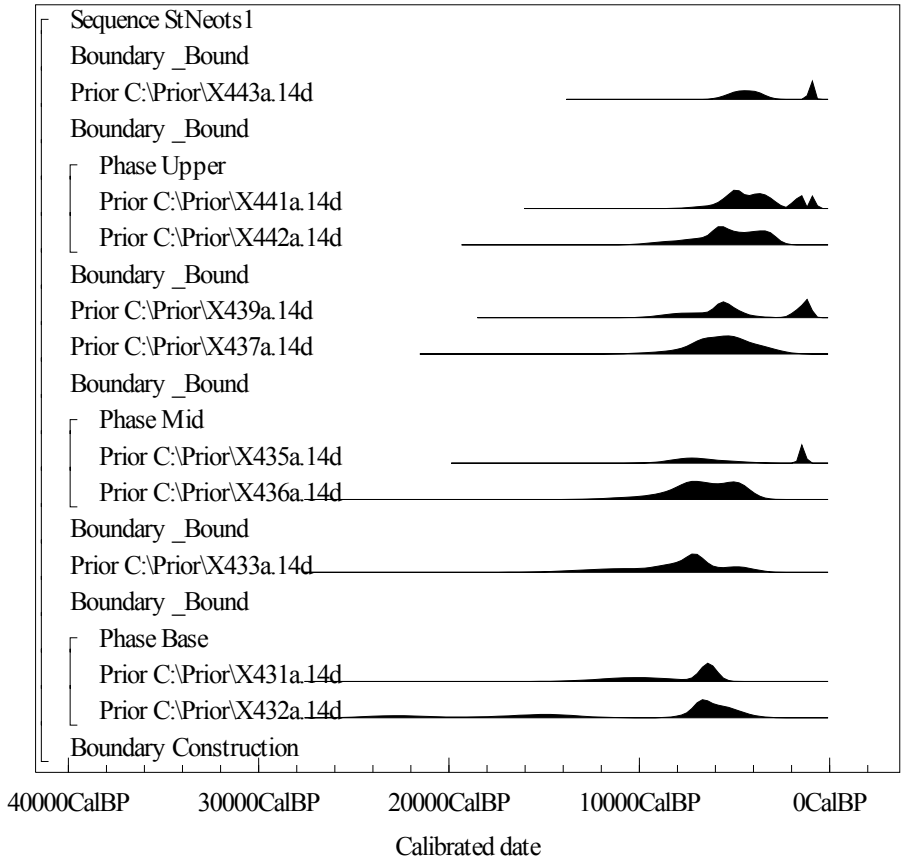

Figure 13a: Single-grain age distributions from the samples from Section 1, northern cursus, as plotted in Figure 7, as prior distributions within OxCal 3.4

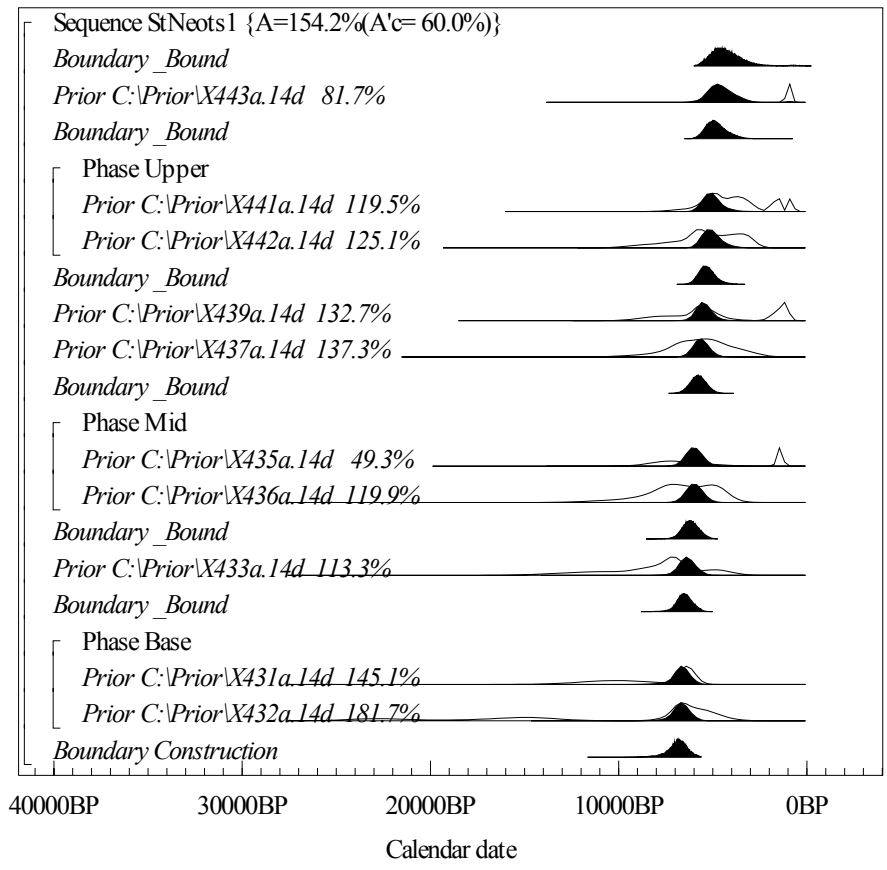

Figure 13b: Bayesian age model and posterior distributions for the data in Figure 13a, Section 1. In both plots, the samples are plotted in the correct stratigraphic order, with replicate samples input as a single phase

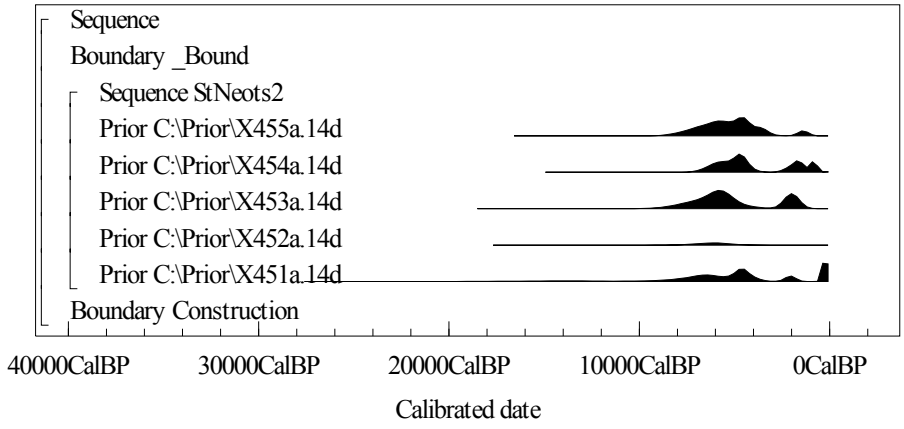

(a)

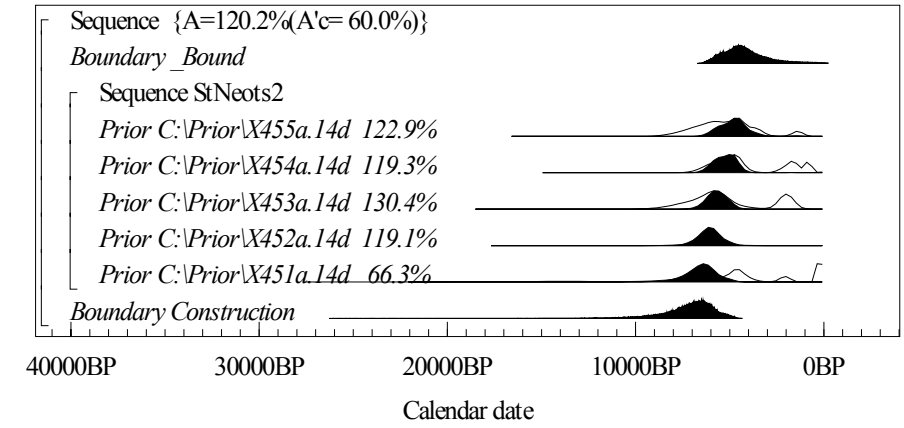

(b)

Figure 14: Plot (a), single grain age distributions from the samples from Section 2, southern cursus, as plotted in Figure 8, as prior distributions within OxCal 3.4. Plot (b), Bayesian age model and posterior distributions for the data in Figure 14a. In both plots, the samples are plotted in the correct stratigraphic order

Table 6 provides the age estimates for each sample, listed in stratigraphic order. These are quoted in the style usual for luminescence data with a central most likely value and the symmetrical 1 sigma uncertainty. This approach is validated for these data by the observation that the posterior distributions approximate Gaussian distributions rather closely (Figs. 13b and 14b). The input and output ranges for each sample are given in Appendix B, as are the calculations for the central values and uncertainties. As mentioned above, both analyses returned high agreement indices of 154% for Section 1 and 119% for Section 2. The fact that these values are both well above the minimum values considered acceptable (60%) or what should be expected to be average values for consistent sequences (100%), suggests that on average the uncertainties are effectively overestimated. This should result in the Bayesian age model results presented below representing conservative uncertainty ranges. Further consideration of dealing with these issues is required in the light of experience with OSL single grain data.

The corresponding data for Section 2, southern cursus, are shown in Figures 14a and b, and included in Appendix B, and the age estimates are included in Table 6.

Conclusions

The first and main conclusion of this study regards the age of the two cursus monuments, and the filling of their ditches. The single grain data suggest that the two features started filling with sediment between the early and mid-fifth millenium BC, and were substantially filled by around the late Neolithic in the early to mid-third millenium BC. This is broadly consistent with previous age estimates based on 6 standard multi-grain OSL measurements made at Sections 2 and 3 (Rhodes 2001; 2002).

The second conclusion regards the specific advantages of the single grains approach over conventional OSL dating. For problematic samples, such as those encountered in Section 1, particularly at the base (X431 and X432), dating based on standard aliquots would return severe overestimates at the base, and underestimates for the upper samples (eg X443), as displayed by the results in Table 4, and Figures 9–12. Small aliquots may overcome some of these problems, though it is not clear from these measurements to what degree they may be systematically offset by dim grain contributions which may have a systematic bias in dose. In particular, the use of a Bayesian approach to combine the data from different samples can provide useful and significant chronological control.

However, the very low yields of grains with useful OSL data versus those measured, approximately 2% for these samples, make this approach time consuming, particularly in terms of machine time and analysis time. Issues regarding the observed variation between single grains, even for laboratory irradiated samples or for the natural doses of grains extracted from pottery, point to the fact that there is further technical and theoretical research to be undertaken in these areas.

Despite these current limitations, the single-grain approach adopted here has the potential not only to provide reliable age estimates for archaeological or environmental contexts where no other techniques may be available, but also can provide information regarding the post-depositional history of the site, including the degree and possibly timing of disturbance such as bioturbation.

Acknowledgements

The author would like to acknowledge the assistance of Laura Willis, Roger Nathan, and Chris Ellis and excavation team with sampling, Jean-Luc Schwenninger and Tom Gurling with sample preparation, and Chris Bronk Ramsey with data interpretation. Wessex Archaeology is thanked for assistance and support at all stages of this project, in particular for providing input for figures, and Alex Bayliss is thanked for assistance in project design and planning, and in editing this report. Mike Allen is thanked for his significant input and encouragement throughout the project. Funding was provided by English Heritage through the Aggregates Levy Sustainability Fund, project A3442. Elements of the text used here are based on the standard Luminescence Dating Laboratory OSL dating report, parts of which were written by Richard Bailey.

Bibliography

Adamiec, G, 2000 Aspects of pre-dose and other luminescence phenomena in quartz absorbed dose estimation, unpubl DPhil thesis, Univ of Oxford

Adamiec, G, and Aitken, M J, 1998 Dose-rate conversion factors: update. *Ancient TL*, **16**, 37–50

Aitken, M J, 1985 *Thermoluminescence dating,* London, (Academic Press)

Aitken, M J, 1998 *Introduction to optical dating,* Oxford (Oxford University Press)

Allen, M J, Rhodes, E J, Beavan, N, and Groves, C, 2004 Absolute chronology, in *A prehistoric ritual complex at Eynesbury, Cambridshire* (ed C J Ellis), East Anglian Archaeology Occassional Papers, **17**, 60–8

Bailey, R M, 2001 Towards a general kinetic model for optically and thermally stimulated luminescence of quartz, *Radiation Measurements*, **33**, 17–45

Bailey, R M, 2000 Circumventing possible inaccuracies of the single aliquot regeneration method for the optical dating of quartz, *Radiation Measurements*, **32**, 833–40

Bøtter-Jensen, L, Bulur, E, Duller, G A T, and Murray, A S, 2000 Advances in luminescence instrument systems, *Radiation Measurements*, **32**, 523–8

Bronk Ramsey, C, 1995 Radiocarbon Calibration and Analysis of Stratigraphy: The OxCal Program, *Radiocarbon*, **37**(2), 425–30

Henshilwood, C S, d'Errico, F, Yates, R, Jacobs, Z, Tribolo, C, Duler, G A T, Mercier, N, Sealy, J C, Valladas, H, Watts, I, and Wintle, A G, 2002 Emergence of modern human behaviour: Middle Stone Age engravings from South Africa, *Science*, **295**, 1278–80

Huntley, D J, Godfrey-Smith, D I, and Thewalt, M L W, 1985 Optical dating of sediments, *Nature*, **313**, 105–7

Mejdahl, V, 1979 Thermoluminescence dating: beta dose attenuation in quartz grains, *Archaeometry,* **21**, 61–73

Murray, A S, and Wintle, A G, 2000 Luminescence dating of quartz using an improved single-aliquot regenerative-dose protocol, *Radiation Measurements*, **32**, 57–73

Nathan, R P, Thomas, P J, Jain, M, Murray, A S, and Rhodes, E J, 2003 Environmental dose rate heterogeneity of beta radiation and its implications for luminescence dating: Monte Carlo modelling and experimental validation, *Radiation Measurements*, **37**, 305–13

Olley, J, Caitcheon, G, and Murray, A S, 1998 The distribution of apparent dose as determined by optically stimulated luminescence in small aliquots of fluvial quartz: Implications for dating young sediments, *Quaternary Geochronology (Quaternary Sci Reviews)*, **17**, 1033–40

Olley, J, Caitcheon, G, and Roberts, R G, 1999 The origin of dose distribution in fluvial sediments, and the prospect of dating single grains from fluvial deposits using optically stimulated luminescence. *Radiation Measurements*, **30**, 207–17

Owen, L A, Mitchell, W A, Bailey, R M, Coxon, P, and Rhodes, E J, 1997 Style and timing of glaciation in the Lahul Himalaya, northern India: a frame work for reconstructing Late Quaternary palaeoclimatic change in the western Himalayas, *J Quaternary Sci*, **12**, 83–109

Prescott, J R, and Hutton, J T, 1994 Cosmic ray contributions to dose rates for luminescence and ESR dating: large depths and long term time variations, *Radiation Measurements*, **23**, 497–500

Rhodes, E J, 1988 Methodological considerations in the optical dating of quartz, *Quaternary Sci Reviews*, **7**, 395–400

Rhodes, E J, 2001 *Optically Stimulated Luminescence dating report; P064 St Neots Cursus*, Unpubl report for Wessex Archaeol

Rhodes, E J, 2002 *Optically Stimulated Luminescence dating report; P064 St Neots Cursus; additional data*, Unpubl report for Wessex Archaeol

Rhodes, E J, Bronk-Ramsey, C, Outram, Z, Batt, C, Willis, L, Dockrill, S, Batt, C, and Bond, J, 2003 Bayesian methods applied to the interpretation of multiple OSL dates: high precision sediment age estimates from Old Scatness Broch excavations, Shetland Isles, *Quaternary Sci Reviews*, **22**, 1231–44

Roberts, R, Bird, M, Olley, J, Galbraith, R, Lawson, E, Laslett, G, Yoshida, H, Jones, R, Fullagar, R, Jacobsen, G, and Hua, Q, 1998 Optical and radiocarbon dating at Jinmium rock shelter in northern Australia, *Nature*, **393**, 358–62

Roberts, R G, Galbraith, R F, Olley, J M, Yoshida, H, and Laslett G M, 1999 Optical dating of single and multiple grains of quartz from jinmium rock shelter, northern Australia, part 2, Results and implications, *Archaeometry*, **41**, 365–95

Smith, B W, Aitken, M J, Rhodes, E J, Robinson, P D, and Geldard, D M, 1986 Optical dating: methodological aspects, *Radiation Protection Dosimetry*, **17**, 229–33

Smith, B W, Rhodes, E J, Stokes, S, Spooner, N A, and Aitken, M J, 1990 Optical dating of sediments: initial results from Oxford, *Archaeometry*, **32**, 19–31

Stokes, S, Thomas, D S G, and Washington, R W, 1997 Multiple episodes of aridity in southern Africa since the last interglacial period, *Nature*, **388**, 154–9

Truscott, A J, Duler, G A T, Bøtter-Jensen, L, Murray, A S, and Wintle, A G, 2000 Reproducibility of optically stimulated luminescence measurements from single grains of Al_2O_3:C and annealed quartz, *Radiation Measurements*, **32**, 447–51

Appendix A – Luminescence dating

The physical basis of luminescence dating

When ionising radiation (predominantly alpha, beta, or gamma radiation) interacts with an insulating crystal lattice (such as quartz or feldspar), a net redistribution of electronic charge takes place. Electrons are stripped from the outer shells of atoms and though most return immediately, a proportion escape and become trapped at meta-stable sites within the lattice. This charge redistribution continues for the duration of the radiation exposure and the amount of trapped charge is therefore related to both the duration and intensity of radiation exposure.

Even though trapped at meta-stable sites, electrons become 'free' once again under certain conditions (eg if the crystal is heated and/or illuminated). Once liberated a free electron may become trapped once again or may return to a vacant position caused by the absence of a previously displaced electron (a 'hole'). This latter occurrence is termed 'recombination' and the location of the hole is described as the 'recombination centre'. As recombination occurs, a proportion of the energy of the electron is dissipated. Depending upon the nature of the centre where recombination occurs, this energy is expelled as heat and/or light. When the crystal grain is either heated or illuminated following irradiation (the 'dose') the total amount of light emitted (luminescence) is therefore directly related to the number of liberated electrons and available recombination sites. This is the fundamental principle upon which luminescence dating is based.

In cases where the duration of dosing is not known (as is the case for dating), estimates can be made from laboratory measurements. The response (the sensitivity) of the sample to radiation dose (ie the amount of light observed for a given amount of laboratory radiation, usually β-radiation) must be established. From this relationship the equivalent radiation exposure required to produce the same amount of light as that observed following the environmental dose can be determined, and is termed the 'equivalent dose' (D_e). The D_e (measured in Gy) is therefore an estimate of the total dose absorbed during the irradiation period. When the dose rate (the amount of radiation per unit time, measured in μGy/a) is measured (or calculated from measured concentrations of radionuclides), the duration of the dosing period can be calculated using the equation:

$$\text{Duration of dosing period} = D_e / \text{dose rate.}$$

The technique of optical dating was first applied to quartz by Huntley *et al* (1985), and methodological details were further developed by Smith *et al* (1986) and Rhodes (1988). The technique was demonstrated to work well for aeolian samples by Smith *et al* (1990), and has further proved to provide useful age estimates for a range of sedimentary contexts ranging from aeolian (eg Stokes *et al* 1997) to glacial contexts (Owen *et al* 1997). Further developmental research has introduced D_e measurement protocols that use a 'single aliquot regenerative-dose' (SAR) protocol. These protocols have the potential to provide increased precision in the luminescence measurements, and may in some cases provide an indication of incomplete zeroing of the luminescence signal at the time of deposition.

The Single Aliquot Regenerative-Dose (SAR) protocol

The SAR method is a regeneration procedure where the light level of the natural signal is converted into Gy via an interpolation between regenerated (ie known dose) points. The natural and regenerated signals are measured using the same aliquot. Sensitivity change commonly observed in quartz TL/OSL has previously precluded meaningful results being obtained this way. A key development reported by Murray and Wintle (2000) is that sample (aliquot) sensitivity is monitored following each OSL measurement (L_i) using the OSL

response to a common test dose (S_i). Plots of $OSL1_i/OSL2_i$ provide the necessary (sensitivity change corrected) data for interpolation. The procedure is further outlined below, in Figure A1.

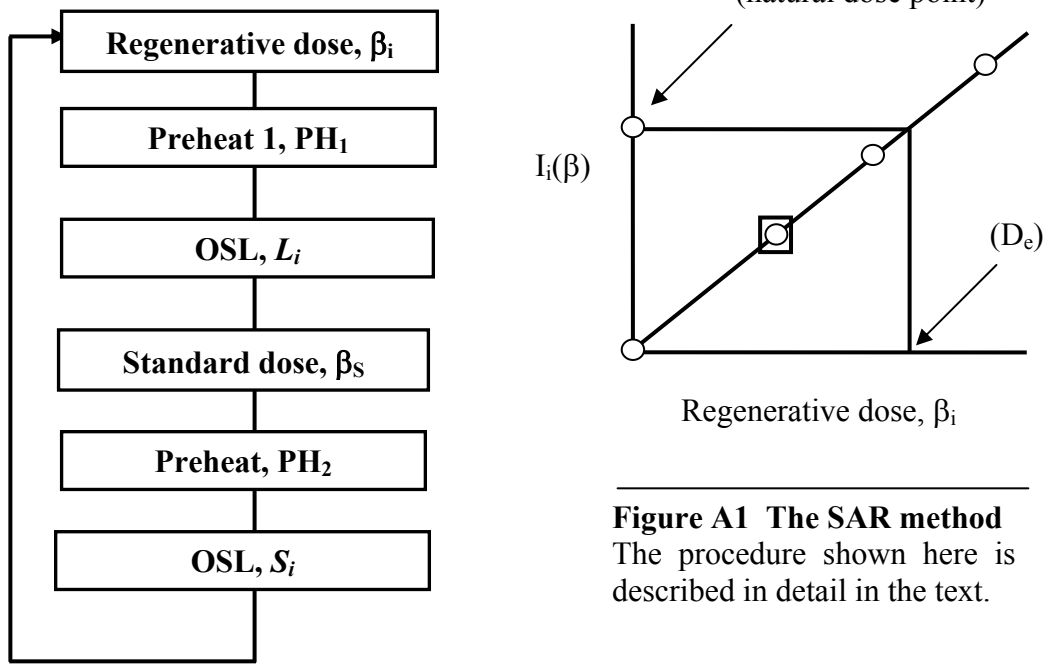

Figure A1 The SAR method
The procedure shown here is described in detail in the text.

Steps 1-6 are repeated n times in order to produce the data points required for interpolation (the first dose β_1 being zero, to give a measure of the natural signal). Typically n=7 (ie the natural plus 6 regeneration points, including one zero dose point and one repeat point). PH_1 and PH_2 are usually different although Wintle and Murray (2000) report no dependence of D_e on either (over the range of 200–280°C). The OSL signal is integrated over the initial part of the decay (to ~10% of initial intensity) and the background is taken as the light level measured at the end of the OSL measurement.

Wintle and Murray (2000) have introduced two further steps in to the measurement procedure. The first is the re-measurement of the first regenerated data point (indicated by the box in the explanatory Figure A1 above). The ratio of the two points (the "recycling ratio") provides an assessment of the efficacy of the sensitivity correction and the accuracy of the technique (large differences being suggestive of an ineffective technique). The second additional step is a measurement of the regenerated OSL due to zero dose. This value gives a measure of the degree of thermal transfer (to the trap(s) responsible for OSL) during preheating. The ratio of this value to the natural OSL value (both corrected for sensitivity change) gives the "thermal transfer ratio" and this is typically in the range of 0.005–0.020. The "recycling ratio" (ideally unity) is typically in the range 0.95–1.05.

Error calculation

This section applies to the standard luminescence age estimates, but not the output of the Bayesian age models, for which the error estimation has additional complexity, discussed by Rhodes *et al* (2003).

The calculated age depends on the estimate of total absorbed dose (D_e) and the annual dose rate (D_R). Both of these estimates have uncertainties associated with them. This section gives general details of how the 'error' (the statistical uncertainty) is calculated for each term and combined with the errors on other terms to give an overall estimate of uncertainty on the estimate of age.

D_e estimation

As described in a previous section (Figure A1), individual estimates of D_e are obtained from each of the aliquot (sub-samples) measured, using the SAR technique. The value (D_e) is obtained by interpolating between the points of the dose response curve. Statistical uncertainties are calculated for each of the individual points and also on the interpolated value of D_e. Typically, 12 aliquots are measured for each sample.

Each of the points on the growth curve is defined as

$$I(\beta)_i = \frac{L_i - f \cdot l_i}{S_i - f \cdot s_i \cdot} \qquad \text{Eq 1}$$

where L_i is the integrated (initial) OSL from the regeneration dose and l_i is the measured background signal, S_i is the integrated (initial) OSL from the test dose and si is the background; f is a scaling factor included to take account of the difference in duration of the L_i *and* S_i, and l_i *and* s_i measurements.

The error on each dose-response data point (see Figure A1) is calculated by propagating 'counting statistics' errors (assuming Poisson statistics) from the integration of raw OSL data. The error on each term in Equation 1 is given by the square-root of the value. For example, the range for L_i is given by $L_i \pm \sqrt{L_i}$. The errors on each value are propagated in the standard way (see below) to give the uncertainty of $I(\beta)_i$.

In cases where the dose response can be (locally) approximated by a straight line, a weighted least squares linear fit is used. The errors in this case are calculated analytically.

In cases where the dose response is significantly non-linear, a single saturating exponential function is used to describe the dose response (a Simplex algorithm is used for fitting in this case). Occasionally an extra linear term is added to the exponential term in order to better describe the form of the dose response, although this is not commonly necessary. The uncertainty for non-linear fitting is calculated using a Monte-Carlo method in which 'random samples' of the dose response data are taken (assuming normally distributed probabilities) and used to obtain a D_e value. The spread in these values is then used to calculate the error on the mean D_e for each aliquot, giving a range for each D_e of $D_{ei} \pm \sigma D_{ei}$

Once the individual D_e values have been obtained from each aliquot (and the associated uncertainties calculated) the values are grouped to give a final overall estimate of D_e. The final estimate (D_e) is calculated using a weighted average. The weight of each D_e is referred to as w_i and defined as

$$w_i = \frac{1}{\sigma D_{ei}{}^2} \Big/ \sum_i \frac{1}{\sigma D_{ei}{}^2} \qquad \text{Eq 2}$$

The weighted mean is defined

$$\overline{D}_e = \sum_i D_{ei} \cdot w_i \qquad \text{Eq 3}$$

The weighted standard error, $\hat{\sigma}_{\bar{x}w}$, is calculated from

$$\hat{\sigma}_{\bar{x}w} = \sqrt{\frac{\sum_i w_i \left(D_{ei} - \overline{D}_e\right)}{1 - \frac{1}{n}}} \Big/ \sqrt{n} \qquad \text{Eq 4}$$

where n is the number of aliquots. The range of the weighted mean D_e is then defined as

$$\overline{D}_e \pm \hat{\sigma}_{\bar{x}w} \qquad \text{Eq 5}$$

Slight modifications to the approach outlined above are made in special circumstances, though in most cases this description is sufficient.

Dose rate

The errors on the dose rate are due to errors in a range of values, for example, the concentration of U, Th, and K, the water content of the sample. The individual components of the dose rate calculation are shown in Appendix C. The uncertainty on the overall dose rate is calculated by combing the uncertainties according to the standard propagation formula given below.

Age calculation

The calculated age is obtained from dividing the mean D_e (Eq 3) by the total dose rate (Appendix C). The uncertainty on the final age estimate is calculated using the error propagation formula given below. All calculations were performed using software developed within the laboratory.

Standard error propagation

If a calculated value (y) is calculated using a function (f) which contains terms x_1, x_2, x_3.... x_n, then

$$y = f\left(x_1, x_2, x_3 \ldots x_n\right) \qquad \text{Eq 6}$$

Each term (x_i) has an associated uncertainty with a range expressed as $x_i \pm \sigma_{xi}$. The overall error of y can be calculated through the addition of the partial derivatives of y with respect to each term. Formally, this is written as

$$\sigma_y = \sqrt{\sum_i \left(\frac{\partial y}{\partial x_i} \cdot \sigma_{xi} \right)^2} \qquad \text{Eq 7}$$

giving a range for y as $y \pm \sigma_Y$.

Appendix B – Luminescence measurement results and OxCal output

Table B1 – Accepted single grain D_e values for measurements based on 400 grains, Section 1

Sample	De (Gy)	1 sigma uncertainty
X431		
	7.2	0.5
	11.4	2.2
X432		
	6.9	1.2
	18.7	1.4
	8.6	0.5
	7.1	1.5
	8.2	1.2
	29.5	2.0
	18.9	1.8
	21.0	3.3
X433		
	6.2	1.0
	10.6	1.0
	9.1	0.6
	12.4	2.5
	8.9	0.9
	15.4	2.6
X435		
	11.2	1.6
	2.1	0.2
	10.8	1.5
	7.8	1.5
	11.4	2.2
	2.1	0.2
	11.5	1.4
X436		
	6.8	0.9
	7.3	0.9
	9.1	1.7
	10.5	1.8
	9.7	2.0
	9.1	1.2
	12.2	1.6
	15.0	2.5
	11.0	0.9
X437		
	7.7	0.9
	11.2	2.5
	7.8	1.8
	9.7	0.9
	7.0	1.3
	9.2	2.0
	5.0	1.2
X439		
	9.5	1.5
	1.5	0.3
	11.5	1.3
	8.0	0.5
	2.2	0.5
	7.2	1.5
	7.3	0.7
X441		
	1.9	0.1
	5.9	0.8
	6.9	0.7
	4.5	0.6
	1.1	0.2
	5.5	1.0
	7.1	0.4
	0.6	0.0
	9.5	1.2
	7.8	0.6
	7.7	0.7
	5.0	0.7
	2.6	0.2
	7.1	1.3
	5.5	0.6
X442		
	10.1	1.0
	8.3	0.9
	7.3	0.7
	5.7	0.7
	5.8	1.1
	8.5	0.5
	4.6	0.6
	12.4	1.6
X443		
	7.0	1.0
	1.3	0.2
	7.1	0.9
	5.6	0.7

Table B2 – Accepted single grain D_e values for measurements based on 400 grains, Section 2

Sample	De (Gy)	1 sigma uncertainty
X451		
	7.0	1.0
	6.9	0.9
	-2.0	1.0
	21.4	4.1
	10.1	0.8
	0.5	0.1
	3.1	0.4
	-0.1	0.1
	11.2	1.1
	9.2	0.8
	12.3	2.0
	7.0	1.0
	7.0	0.4
X452		
	8.8	1.1
	7.9	0.9
	8.0	1.2
	10.4	1.6
	8.7	0.6
	10.0	0.7
X453		
	9.8	1.7
	8.3	1.8
	2.8	0.6
	8.1	0.8
X454		
	3.1	0.6
	9.5	1.0
	1.2	0.3
	7.3	0.6
	7.5	0.5
	7.6	1.0
	-0.1	0.0
	9.0	0.9
	2.5	0.4
	9.3	1.1
X455		
	9.4	0.9
	10.8	1.0
	9.6	1.5
	7.3	0.5
	8.5	1.8
	9.4	0.6
	6.7	1.2
	7.2	0.5
	8.5	0.7
	6.9	1.1
	5.6	0.5
	12.4	1.0
	10.1	1.5

Table B3 – Accepted single grain D_e values for measurements based on 1600 grains

Sample	De (Gy)	1 sigma uncertainty	Sample	De (Gy)	1 sigma uncertainty
X432			X452		
	6.9	1.2		8.8	1.1
	18.7	1.4		7.9	0.9
	8.6	0.5		8.0	1.2
	7.1	1.5		10.4	1.6
	8.2	1.2		8.7	0.6
	29.5	2.0		10.0	0.7
	18.9	1.8		12.7	1.1
	21.0	3.3		3.6	0.8
	7.9	1.3		9.8	1.0
	9.8	2.4		7.6	1.5
	8.4	0.8		7.8	0.9
	4.8	0.7		10.1	2.3
	7.8	0.7		8.3	1.2
	13.5	1.8		10.0	0.7
	8.4	0.5		14.5	2.7
	1.3	0.2		5.4	0.9
	9.4	1.6		8.8	2.0
	16.5	2.3		1.2	0.3
	13.5	2.7		7.3	0.8
	12.2	2.1		5.8	1.2
	7.8	1.5		5.1	0.7
	9.6	0.8		7.6	1.8
	5.9	0.5		7.3	0.5
	7.5	1.0		7.4	1.8
	9.9	1.1		5.7	1.4
	27.5	2.1		10.5	0.6
	1.5	0.1		7.5	1.0
	17.8	2.0		14.5	2.1
	22.4	2.5		8.8	2.0
				10.4	1.2
X443				11.3	1.4
	7.0	1.0		6.8	0.8
	1.3	0.2		6.7	1.1
	7.1	0.9		7.6	0.7
	5.6	0.7		6.6	1.2
	7.2	0.8		7.7	1.3
	11.2	0.9		7.2	1.5
	6.7	0.9		9.8	1.5
	2.3	0.3		8.5	1.6
	2.2	0.2		10.9	1.8
	5.7	1.3			
	3.4	0.6			
	6.9	0.6			
	8.8	0.5			
	12.6	2.3			
	6.1	1.4			
	1.4	0.3			
	11.8	1.5			
	6.8	1.4			
	0.9	0.2			
	12.7	2.7			
	4.5	0.8			
	7.8	0.7			
	6.1	0.5			
	6.7	0.5			
	2.7	0.4			
	10.0	1.7			
	1.7	0.3			
	2.8	0.2			
	9.9	1.1			
	8.3	0.9			
	17.2	1.9			
	2.8	0.3			
	13.1	1.5			

Table B4 – D_e values for measurements based on small aliquots

Sample	De (Gy)	1 sigma uncertainty
X431		
	9.7	0.8
	17.5	5.0
	-2.1	7.0
	16.9	3.4
	3.9	0.6
	6.1	1.2
	10.6	4.0
	21.8	2.7
	8.7	2.8
	29.8	4.0
	14.8	3.7
	2.0	1.1
X432		
	13.8	2.0
	8.7	0.7
	9.2	0.9
	7.1	0.6
	6.0	0.6
	10.5	1.1
	10.5	0.9
	19.9	1.4
	13.8	1.4
	8.9	0.6
	8.8	0.6
	15.1	1.5
X443		
	9.1	0.7
	4.7	0.6
	6.2	0.4
	4.1	0.5
	5.7	0.4
	9.8	0.7
	6.3	0.5
	4.7	0.7
	3.8	0.5
	7.8	0.6
	6.0	0.5
	5.2	0.5
X452		
	8.9	0.6
	10.7	0.7
	8.9	0.8
	9.2	1.2
	8.8	0.5
	7.8	0.4
	8.5	0.7
	10.2	1.8
	7.3	0.8
	6.4	0.5
	10.6	0.7
	10.1	0.7

Table B5 – Single aliquot D_e values for measurements based on standard aliquots

Sample	De (Gy)	1 sigma uncertainty	Sample	De (Gy)	1 sigma uncertainty
X431			X445		
	20.1	1.2		8.3	1.2
	13.0	0.9		9.3	0.7
	17.1	1.4		8.6	0.9
	10.0	0.6		9.4	0.7
	17.6	1.3		9.4	0.9
	16.8	1.1		8.5	0.5
	15.0	0.9		9.5	0.5
	20.2	1.0		10.5	0.7
	16.6	1.7		10.1	0.8
	27.4	1.5		8.8	0.8
	14.3	1.2		9.2	0.8
	18.7	1.6		8.9	0.5
X432			X451		
	7.9	0.7		9.0	1.0
	12.7	0.7		8.5	0.7
	5.5	0.5		10.3	0.7
	17.5	1.1		9.3	0.5
	17.2	1.0		9.5	0.5
	10.7	1.2		9.5	0.7
	17.4	1.4		9.9	0.6
	12.2	0.6		9.4	0.5
	12.9	0.8		8.9	0.6
	2.2	0.1		10.6	0.7
	14.2	1.2		11.9	0.8
	11.0	0.7		9.9	0.6
X443			X453		
	5.9	0.4		7.3	0.5
	4.1	0.3		5.2	0.3
	5.5	0.4		7.6	0.4
	5.2	0.4		7.2	0.5
	5.7	0.4		7.3	0.4
	4.2	0.3		8.3	0.5
	8.9	0.5		4.8	0.3
	5.6	0.4		7.5	0.5
	3.4	0.4		7.5	0.5
	6.3	0.4		7.5	0.5
	4.2	0.2		7.0	0.4
	6.4	0.4		6.9	0.4
X452			X454		
	7.9	0.5		7.2	0.5
	9.3	0.6		7.5	0.5
	7.9	0.4		8.6	0.6
	8.8	0.5		6.7	0.4
	9.1	0.5		9.4	0.5
	8.8	0.4		7.6	0.5
	8.3	0.4		6.0	0.3
	8.5	0.5		6.7	0.4
	8.2	0.5		7.9	0.4
	8.9	0.5		8.6	0.5
	8.7	0.5		8.9	0.5
	8.9	0.5		6.3	0.6
			X455		
				7.4	0.4
				7.9	0.5
				7.7	0.5
				7.4	0.5
				6.9	0.4
				5.2	0.4
				6.9	0.5
				6.7	0.4
				7.2	0.5
				7.6	0.4
				7.1	0.5
				8.0	0.4

Table B6 – Section 1 OxCal input and output ranges

StNeotsSeq1AC input/output ranges

Sample

Input ranges	1 sigma		2 sigma	
C:\Prior\X431a.14d	-9500	-3500	-11500	-3000
C:\Prior\X432a.14d	-14200	-2000	-23000	-1400
C:\Prior\X433a.14d	-7500	-2000	-11700	-1600
C:\Prior\X435a.14d	-6500	1000	-7500	1500
C:\Prior\X436a.14d	-6000	-2400	-9000	-1500
C:\Prior\X437a.14d	-5300	-1900	-7500	0
C:\Prior\X439a.14d	-5000	1500	-7500	1500
C:\Prior\X441a.14d	-3600	600	-5000	1500
C:\Prior\X442a.14d	-4400	-1000	-7500	0
C:\Prior\X443a.14d	-3200	1300	-4000	1500

OxCal output ranges

@_Bound	-5600	-4400	-7200	-3800
@C:\Prior\X431a.14d	-5400	-4200	-6700	-3600
@C:\Prior\X432a.14d	-5400	-4300	-6300	-3700
@_Bound	-5200	-4100	-6000	-3500
@C:\Prior\X433a.14d	-5100	-3900	-5700	-3300
@_Bound	-4900	-3800	-5400	-3200
@C:\Prior\X435a.14d	-4700	-3500	-5200	-3000
@C:\Prior\X436a.14d	-4600	-3500	-5100	-3000
@_Bound	-4400	-3300	-4900	-2800
@C:\Prior\X437a.14d	-4200	-3100	-4700	-2600
@C:\Prior\X439a.14d	-4000	-3000	-4500	-2400
@_Bound	-3900	-2800	-4300	-2200
@C:\Prior\X441a.14d	-3700	-2500	-4000	-1800
@C:\Prior\X442a.14d	-3700	-2500	-4100	-1800
@_Bound	-3400	-2200	-3900	-1400
@C:\Prior\X443a.14d	-3200	-1800	-3700	-1100
@_Bound	-3100	-1400	-4000	2000

Table B7 – Section 2 OxCal input and output ranges

StNeotsSeq2AA input/output ranges

Sample

Input ranges	1 sigma		2 sigma	
C:\Prior\X451a.14d	-5500		-13600	
C:\Prior\X452a.14d	-5200	-3200	-6400	-2200
C:\Prior\X453a.14d	-5500	500	-7000	1000
C:\Prior\X454a.14d	-4500	1500	-5000	2000
C:\Prior\X455a.14d	-5000	-1900	-6500	1000

OxCal output ranges

@_Bound	-6200	-3700	-9500	-2500
@C:\Prior\X451a.14d	-5400	-3700	-6500	-2800
@C:\Prior\X452a.14d	-4800	-3500	-5500	-2800
@C:\Prior\X453a.14d	-4400	-3100	-4900	-2500
@C:\Prior\X454a.14d	-4000	-2600	-4500	-2200
@C:\Prior\X455a.14d	-3700	-2100	-4500	-1300
@_Bound	-3800	-1400	-4500	1000

Table B8 – Section 1 and 2 OxCal midpoint and error calculation for age model data

StNeotsSeq1AC	1sig ranges		2 sig ranges		1sigma			2 sigma		
					centre	error	frac error	centre	error	frac error
@_Bound	-5600	-4400	-7200	-3800	-5000	600	0.09	-5500	1700	0.23
@C:\Prior\X431a.14d	-5400	-4200	-6700	-3600	-4800	600	0.09	-5150	1550	0.22
@C:\Prior\X432a.14d	-5400	-4300	-6300	-3700	-4850	550	0.08	-5000	1300	0.19
@_Bound	-5200	-4100	-6000	-3500	-4650	550	0.08	-4750	1250	0.19
@C:\Prior\X433a.14d	-5100	-3900	-5700	-3300	-4500	600	0.09	-4500	1200	0.18
@_Bound	-4900	-3800	-5400	-3200	-4350	550	0.09	-4300	1100	0.17
@C:\Prior\X435a.14d	-4700	-3500	-5200	-3000	-4100	600	0.10	-4100	1100	0.18
@C:\Prior\X436a.14d	-4600	-3500	-5100	-3000	-4050	550	0.09	-4050	1050	0.17
@_Bound	-4400	-3300	-4900	-2800	-3850	550	0.09	-3850	1050	0.18
@C:\Prior\X437a.14d	-4200	-3100	-4700	-2600	-3650	550	0.10	-3650	1050	0.19
@C:\Prior\X439a.14d	-4000	-3000	-4500	-2400	-3500	500	0.09	-3450	1050	0.19
@_Bound	-3900	-2800	-4300	-2200	-3350	550	0.10	-3250	1050	0.20
@C:\Prior\X441a.14d	-3700	-2500	-4000	-1800	-3100	600	0.12	-2900	1100	0.22
@C:\Prior\X442a.14d	-3700	-2500	-4100	-1800	-3100	600	0.12	-2950	1150	0.23
@_Bound	-3400	-2200	-3900	-1400	-2800	600	0.13	-2650	1250	0.27
@C:\Prior\X443a.14d	-3200	-1800	-3700	-1100	-2500	700	0.16	-2400	1300	0.30
@_Bound	-3100	-1400	-4000	2000	-2250	850	0.20	-1000	3000	1.00

StNeotsSeq2AA	1sig ranges		2 sig ranges		1sigma			2 sigma		
					centre	error	frac error	centre	error	frac error
@_Bound	-6200	-3700	-9500	-2500	-4950	1250	0.18	-6000	3500	0.44
@C:\Prior\X451a.14d	-5400	-3700	-6500	-2800	-4550	850	0.13	-4650	1850	0.28
@C:\Prior\X452a.14d	-4800	-3500	-5500	-2800	-4150	650	0.11	-4150	1350	0.22
@C:\Prior\X453a.14d	-4400	-3100	-4900	-2500	-3750	650	0.11	-3700	1200	0.21
@C:\Prior\X454a.14d	-4000	-2600	-4500	-2200	-3300	700	0.13	-3350	1150	0.21
@C:\Prior\X455a.14d	-3700	-2100	-4500	-1300	-2900	800	0.16	-2900	1600	0.33
@_Bound	-3800	-1400	-4500	1000	-2600	1200	0.26	-1750	2750	0.73

Appendix C – Dose rate calculation and multi-grain age estimation

The following section contains ages estimates with age release codes (OxL- numbers) for the six multigrain standard aliquot samples already dated for Wessex Archaeology (Rhodes 2001, 2002). These are samples X451, X452, X453, X454, X455, and X445. The table contains the measured dose, and dose rate values, and provides the age estimate and associated uncertainty calculated.

Also included are the small aliquot equivalent dose values and the standard equivalent dose values for samples X431, X432, X443, and X452. The table contains the measured dose, and dose rate values, and provides the age estimate and associated uncertainty calculated for these samples. No Age estimate release codes are provided, as this work is primarily experimental in nature.

For the further samples, only single-grain equivalent dose distributions were measured. For these samples, the following tables are used to calculate the correct dose rate, while no single equivalent dose value is meaningful. These samples have a value of 1.00 input for the equivalent dose, and the age shown is therefore meaningless, and should not be interpreted as the correct age for these samples.

These tables are based on a spreadsheet modified from one written by Richard Bailey, and provide a rigorous estimation of dose rate contributions as described in the text and a rigorous combination of all the different error terms.

Appendix C

Sample number	SNC01-21	SNC01-22	SNC01-22	SNC01-23	SNC01-24	SNC01-25
Laboratory code	X451	X452	X452	X453	X454	X455
Age estimate code	OxL-1188	OxL-1189	small	OxL-1190	OxL-1191	OxL-1192
De (Gy)	9.51	8.60	8.42	7.41	7.83	7.34
uncertainty	0.27	0.22	0.42	0.19	0.35	0.26
measured	0.19	0.13	0.38	0.12	0.31	0.21
0.020	0.190	0.172	0.168	0.148	0.157	0.147
Grain size						
Min. grain size (μm)	125	125	125	125	125	125
Max grain size (μm)	180	180	180	180	180	180
External gamma-dose (mGy/a)	0.491	0.543	0.573	0.604	0.620	0.620
error	0.004	0.005	0.005	0.005	0.005	0.005
Measured concentrations						
standard fractional error	0.050	0.050	0.050	0.050	0.050	0.050
% K	1.010	0.835	0.835	0.675	0.958	0.930
error (%K)	0.018	0.018	0.017	0.017	0.017	0.017
Th (ppm)	6.930	6.600	6.600	5.130	6.250	5.990
error (ppm)	0.185	0.186	0.187	0.188	0.188	0.188
U (ppm)	1.280	1.020	1.020	1.480	1.200	1.330
error (ppm)	0.094	0.092	0.090	0.089	0.088	0.088
Cosmic dose calculations						
Depth (m)	1.100	1.000	1.000	0.900	0.880	0.810
error (m)	0.100	0.100	0.100	0.100	0.100	0.100
Average overburden density (g.cm^3)	1.900	1.900	1.900	1.900	1.900	1.900
error (g.cm^3)	0.100	0.100	0.100	0.100	0.100	0.100
Latitude (deg.), north positive	52	52	52	52	52	52
Longditude (deg.), east positive	0	0	0	0	0	0
Altitude (m above sea-level))	10	10	10	10	10	10
Cosmic dose rate (mGy/a)	0.182	0.184	0.184	0.187	0.187	0.189
error	0.021	0.023	0.023	0.025	0.025	0.027
Moisture content						
Moisture (water / wet sediment)	0.150	0.150	0.150	0.150	0.150	0.150
error	0.050	0.050	0.050	0.050	0.050	0.050
Total dose rate (mGy/a)	**1.55**	**1.46**	**1.49**	**1.45**	**1.63**	**1.62**
error (mGy/a)	**0.07**	**0.06**	**0.06**	**0.06**	**0.07**	**0.07**
% error	**4.79**	**4.40**	**4.30**	**4.02**	**4.40**	**4.40**
AGE (a)	**6147**	**5885**	**5643**	**5112**	**4809**	**4526**
error (a)	**342**	**298**	**370**	**244**	**300**	**254**
% error	**5.56**	**5.06**	**6.55**	**4.77**	**6.25**	**5.62**
years AD/BC	-4144	-3882	-3640	-3109	-2806	-2523

Sample number Laboratory code Age estimate code	SNC01-21 X451 OxL-1188	SNC01-22 X452 OxL-1189	SNC01-22 X452 small	SNC01-23 X453 OxL-1190	SNC01-24 X454 OxL-1191	SNC01-25 X455 OxL-1192
Average beta-attenuation						
standard fractional error	0.050	0.050	0.050	0.050	0.050	0.050
Natural U	0.877	0.877	0.877	0.877	0.877	0.877
error	0.044	0.044	0.044	0.044	0.044	0.044
Th-232	0.822	0.822	0.822	0.822	0.822	0.822
error	0.041	0.041	0.041	0.041	0.041	0.041
K-40	0.946	0.946	0.946	0.946	0.946	0.946
error	0.047	0.047	0.047	0.047	0.047	0.047
Dose rate conversion (mGy/a)						
standard fractional error	0.050	0.050	0.050	0.050	0.050	0.050
U (ppm)						
Beta	0.146	0.146	0.146	0.146	0.146	0.146
error	0.007	0.007	0.007	0.007	0.007	0.007
Gamma	0.000	0.000	0.000	0.000	0.000	0.000
error	0.000	0.000	0.000	0.000	0.000	0.000
Th (ppm)						
Beta	0.027	0.027	0.027	0.027	0.027	0.027
error	0.001	0.001	0.001	0.001	0.001	0.001
Gamma	0.000	0.000	0.000	0.000	0.000	0.000
error	0.000	0.000	0.000	0.000	0.000	0.000
K (%)						
Beta	0.782	0.782	0.782	0.782	0.782	0.782
error	0.039	0.039	0.039	0.039	0.039	0.039
Gamma	0.000	0.000	0.000	0.000	0.000	0.000
error	0.000	0.000	0.000	0.000	0.000	0.000
Cosmic dose						
Geomagnetic latitude	54.7	54.7	54.7	54.7	54.7	54.7
Dc (mGy/a), 55N G.lat, 0 km Alt.	0.181	0.184	0.184	0.186	0.187	0.189
error	0.021	0.023	0.023	0.025	0.025	0.027
Moisture						
F	0.420	0.420	0.420	0.420	0.420	0.420
error	0.099	0.099	0.099	0.099	0.099	0.099
W	0.420	0.420	0.420	0.420	0.420	0.420
error	0.099	0.099	0.099	0.099	0.099	0.099
WF	0.176	0.176	0.176	0.176	0.176	0.176
error	0.059	0.059	0.059	0.059	0.059	0.059
Age uncertainties	1.000	1.000	1.000	1.000	1.000	1.000
dDR/K	0.606	0.606	0.606	0.606	0.606	0.606
dDR/dC(B, K)	0.783	0.647	0.647	0.523	0.743	0.721
dDR/dA(K)	0.647	0.535	0.535	0.432	0.614	0.596
dDR/dTh	0.018	0.018	0.018	0.018	0.018	0.018
dDR/dC(B, Th)	4.667	4.444	4.444	3.454	4.209	4.034
dDR/dA(Th)	0.155	0.148	0.148	0.115	0.140	0.134
dDR/dU	0.105	0.105	0.105	0.105	0.105	0.105
dDR/dC(B, U)	0.719	0.719	0.719	0.719	0.719	0.719
dDR/dA(U)	0.153	0.122	0.122	0.177	0.144	0.159
dDR/dW	-0.376	-0.316	-0.316	-0.283	-0.353	-0.350
dDR/dF	-0.376	-0.316	-0.316	-0.283	-0.353	-0.350
dDR/C(G, K)	0.841	0.695	0.695	0.562	0.798	0.774
dDR/C(G, Th)	5.769	5.495	5.495	4.271	5.203	4.987
dDR/dC(G, U)	1.066	0.849	0.849	1.232	0.999	1.107
dDR/dCosmic	1.000	1.000	1.000	1.000	1.000	1.000
Dage/dDe	0.646	0.684	0.670	0.690	0.614	0.617
Dage/dDR	-3.974	-4.027	-3.782	-3.526	-2.953	-2.790

Appendix C

Sample number	SNC01-15
Laboratory code	X445
Age estimate code	OxL-1193
De (Gy)	9.24
uncertainty	0.26
measured	0.18
0.020	0.185
Grain size	
Min. grain size (μm)	125
Max grain size (μm)	180
External gamma-dose (mGy/a)	0.429
error	0.004
Measured concentrations	
standard fractional error	0.050
% K	1.020
error (%K)	0.018
Th (ppm)	6.590
error (ppm)	0.185
U (ppm)	1.420
error (ppm)	0.094
Cosmic dose calculations	
Depth (m)	1.000
error (m)	0.100
Average overburden density (g.cm^3)	1.900
error (g.cm^3)	0.100
Latitude (deg.), north positive	52
Longditude (deg.), east positive	0
Altitude (m above sea-level))	10
Cosmic dose rate (mGy/a)	0.184
error	0.023
Moisture content	
Moisture (water / wet sediment)	0.150
error	0.050
Total dose rate (mGy/a)	**1.50**
error (mGy/a)	**0.08**
% error	**5.03**
AGE (a)	**6154**
error (a)	**354**
% error	**5.75**
years AD/BC	4420

Sample number Laboratory code Age estimate code	SNC01-15 X445 OxL-1193
Average beta-attenuation	
standard fractional error	0.050
Natural U	0.877
error	0.044
Th-232	0.822
error	0.041
K-40	0.946
error	0.047
Dose rate conversion (mGy/a)	
standard fractional error	0.050
U (ppm)	
Beta	0.146
error	0.007
Gamma	0.000
error	0.000
Th (ppm)	
Beta	0.027
error	0.001
Gamma	0.000
error	0.000
K (%)	
Beta	0.782
error	0.039
Gamma	0.000
error	0.000
Cosmic dose	
Geomagnetic latitude	54.7
Dc (mGy/a), 55N G.lat, 0 km Alt.	0.184
error	0.023
Moisture	
F	0.420
error	0.099
W	0.420
error	0.099
WF	0.176
error	0.059
Age uncertainties	1.000
dDR/K	0.606
dDR/dC(B, K)	0.791
dDR/dA(K)	0.653
dDR/dTh	0.018
dDR/dC(B, Th)	4.438
dDR/dA(Th)	0.147
dDR/dU	0.105
dDR/dC(B, U)	0.719
dDR/dA(U)	0.170
dDR/dW	-0.382
dDR/dF	-0.382
dDR/C(G, K)	0.849
dDR/C(G, Th)	5.486
dDR/dC(G, U)	1.182
dDR/dCosmic	1.000
Dage/dDe	0.666
Dage/dDR	-4.099

Appendix C

Sample number	SNC01-01	SNC01-01	SNC01-02	SNC01-02	SNC01-03
Laboratory code	X431	X431	X432	X432	X433
Age estimate code	std	small	std	small	
De (Gy)	18.29	6.71	12.20	8.32	1.00
uncertainty	0.83	2.18	0.58	0.84	0.19
measured	0.74	2.18	0.53	0.82	0.19
0.020	0.366	0.134	0.244	0.166	0.020
Grain size					
Min. grain size (μm)	125	125	125	125	125
Max grain size (μm)	180	180	180	180	180
External gamma-dose (mGy/a)	0.424	0.424	0.424	0.424	0.495
error	0.003	0.003	0.003	0.003	0.025
Measured concentrations					
standard fractional error	0.050	0.050	0.050	0.050	0.050
% K	0.550	0.550	0.744	0.744	0.651
error (%K)	0.028	0.028	0.037	0.037	0.033
Th (ppm)	4.680	4.680	6.020	6.020	6.420
error (ppm)	0.234	0.234	0.301	0.301	0.321
U (ppm)	1.090	1.090	1.210	1.210	1.080
error (ppm)	0.055	0.055	0.061	0.061	0.054
Cosmic dose calculations					
Depth (m)	1.150	1.150	1.150	1.150	0.990
error (m)	0.050	0.050	0.050	0.050	0.050
Average overburden density (g.cm^3)	1.900	1.900	1.900	1.900	1.900
error (g.cm^3)	0.100	0.100	0.100	0.100	0.100
Latitude (deg.), north positive	52	52	52	52	52
Longditude (deg.), east positive	0	0	0	0	0
Altitude (m above sea-level))	10	10	10	10	10
Cosmic dose rate (μGy/ka)	0.181	0.181	0.181	0.181	0.184
error	0.015	0.015	0.015	0.015	0.016
Moisture content					
Moisture (water / wet sediment)	0.150	0.150	0.150	0.150	0.150
error	0.050	0.050	0.050	0.050	0.050
Total dose rate (mGy/a)	**1.14**	**1.14**	**1.29**	**1.29**	**1.31**
error (mGy/a)	**0.05**	**0.05**	**0.06**	**0.06**	**0.06**
% error	**4.18**	**4.18**	**4.70**	**4.70**	**4.64**
AGE (a)	**16066**	**5894**	**9433**	**6433**	**766**
error (a)	**988**	**1934**	**632**	**714**	**151**
% error	**6.15**	**32.82**	**6.70**	**11.10**	**19.66**
years AD/BC	-14063	-3891	-7430	-4430	1237

Sample number	SNC01-01	SNC01-01	SNC01-02	SNC01-02	SNC01-03
Laboratory code	X431	X431	X432	X432	X433
Age estimate code	std	small	std	small	0
Average beta-attenuation					
standard fractional error	0.050	0.050	0.050	0.050	0.050
Natural U	0.877	0.877	0.877	0.877	0.877
error	0.044	0.044	0.044	0.044	0.044
Th-232	0.822	0.822	0.822	0.822	0.822
error	0.041	0.041	0.041	0.041	0.041
K-40	0.946	0.946	0.946	0.946	0.946
error	0.047	0.047	0.047	0.047	0.047
Dose rate conversion (mGy/a)					
standard fractional error	0.050	0.050	0.050	0.050	0.050
U (ppm)					
Beta	0.146	0.146	0.146	0.146	0.146
error	0.007	0.007	0.007	0.007	0.007
Gamma	0.000	0.000	0.000	0.000	0.000
error	0.000	0.000	0.000	0.000	0.000
Th (ppm)					
Beta	0.027	0.027	0.027	0.027	0.027
error	0.001	0.001	0.001	0.001	0.001
Gamma	0.000	0.000	0.000	0.000	0.000
error	0.000	0.000	0.000	0.000	0.000
K (%)					
Beta	0.782	0.782	0.782	0.782	0.782
error	0.039	0.039	0.039	0.039	0.039
Gamma	0.000	0.000	0.000	0.000	0.000
error	0.000	0.000	0.000	0.000	0.000
Cosmic dose					
Geomagnetic latitude	54.7	54.7	54.7	54.7	54.7
Dc (mGy/a), 55N G.lat, 0 km Alt.	0.180	0.180	0.180	0.180	0.184
error	0.015	0.015	0.015	0.015	0.016
Moisture					
F	0.420	0.420	0.420	0.420	0.420
error	0.099	0.099	0.099	0.099	0.099
W	0.420	0.420	0.420	0.420	0.420
error	0.099	0.099	0.099	0.099	0.099
WF	0.176	0.176	0.176	0.176	0.176
error	0.059	0.059	0.059	0.059	0.059
Age uncertainties	1.000	1.000	1.000	1.000	1.000
dDR/K	0.606	0.606	0.606	0.606	0.606
dDR/dC(B, K)	0.426	0.426	0.577	0.577	0.505
dDR/dA(K)	0.352	0.352	0.477	0.477	0.417
dDR/dTh	0.018	0.018	0.018	0.018	0.018
dDR/dC(B, Th)	3.151	3.151	4.054	4.054	4.323
dDR/dA(Th)	0.105	0.105	0.135	0.135	0.144
dDR/dU	0.105	0.105	0.105	0.105	0.105
dDR/dC(B, U)	0.719	0.719	0.719	0.719	0.719
dDR/dA(U)	0.130	0.130	0.145	0.145	0.129
dDR/dW	-0.230	-0.230	-0.296	-0.296	-0.269
dDR/dF	-0.230	-0.230	-0.296	-0.296	-0.269
dDR/C(G, K)	0.458	0.458	0.619	0.619	0.542
dDR/C(G, Th)	3.896	3.896	5.012	5.012	5.345
dDR/dC(G, U)	0.907	0.907	1.007	1.007	0.899
dDR/dCosmic	1.000	1.000	1.000	1.000	1.000
Dage/dDe	0.878	0.878	0.773	0.773	0.766
Dage/dDR	-14.112	-5.177	-7.294	-4.974	-0.587

Appendix C

Sample number Laboratory code Age estimate code	SNC01-05 X435	SNC01-06 X436	SNC01-07 X437	SNC01-09 X439
De (Gy)	1.00	1.00	1.00	1.00
uncertainty	0.19	0.19	0.19	0.19
measured	0.19	0.19	0.19	0.19
0.020	0.020	0.020	0.020	0.020
Grain size				
Min. grain size (μm)	125	125	125	125
Max grain size (μm)	180	180	180	180
External gamma-dose (mGy/a)	0.541	0.541	0.546	0.550
error	0.027	0.027	0.027	0.028
Measured concentrations				
standard fractional error	0.050	0.050	0.050	0.050
% K	0.841	0.781	0.769	0.673
error (%K)	0.042	0.039	0.038	0.034
Th (ppm)	7.160	7.360	6.840	6.660
error (ppm)	0.358	0.368	0.342	0.333
U (ppm)	1.750	1.720	1.390	1.470
error (ppm)	0.088	0.086	0.070	0.074
Cosmic dose calculations				
Depth (m)	0.850	0.850	0.750	0.670
error (m)	0.050	0.050	0.050	0.050
Average overburden density (g.cm^3)	1.900	1.900	1.900	1.900
error (g.cm^3)	0.100	0.100	0.100	0.100
Latitude (deg.), north positive	52	52	52	52
Longditude (deg.), east positive	0	0	0	0
Altitude (m above sea-level))	10	10	10	10
Cosmic dose rate (μGy/ka)	0.188	0.188	0.190	0.192
error	0.018	0.018	0.019	0.020
Moisture content				
Moisture (water / wet sediment)	0.150	0.150	0.150	0.150
error	0.050	0.050	0.050	0.050
Total dose rate (mGy/a)	**1.55**	**1.52**	**1.47**	**1.43**
error (mGy/a)	**0.08**	**0.07**	**0.07**	**0.07**
% error	**4.89**	**4.80**	**4.78**	**4.63**
AGE (a)	**644**	**659**	**678**	**701**
error (a)	**127**	**130**	**134**	**138**
% error	**19.72**	**19.70**	**19.69**	**19.66**
years AD/BC	1359	1344	1325	1302

Sample number Laboratory code Age estimate code	SNC01-05 X435 0	SNC01-06 X436 0	SNC01-07 X437 0	SNC01-09 X439 0
Average beta-attenuation				
standard fractional error	0.050	0.050	0.050	0.050
Natural U	0.877	0.877	0.877	0.877
error	0.044	0.044	0.044	0.044
Th-232	0.822	0.822	0.822	0.822
error	0.041	0.041	0.041	0.041
K-40	0.946	0.946	0.946	0.946
error	0.047	0.047	0.047	0.047
Dose rate conversion (mGy/a)				
standard fractional error	0.050	0.050	0.050	0.050
U (ppm)				
Beta	0.146	0.146	0.146	0.146
error	0.007	0.007	0.007	0.007
Gamma	0.000	0.000	0.000	0.000
error	0.000	0.000	0.000	0.000
Th (ppm)				
Beta	0.027	0.027	0.027	0.027
error	0.001	0.001	0.001	0.001
Gamma	0.000	0.000	0.000	0.000
error	0.000	0.000	0.000	0.000
K (%)				
Beta	0.782	0.782	0.782	0.782
error	0.039	0.039	0.039	0.039
Gamma	0.000	0.000	0.000	0.000
error	0.000	0.000	0.000	0.000
Cosmic dose				
Geomagnetic latitude	54.7	54.7	54.7	54.7
Dc (mGy/a), 55N G.lat, 0 km Alt.	0.188	0.188	0.190	0.192
error	0.018	0.018	0.019	0.020
Moisture				
F	0.420	0.420	0.420	0.420
error	0.099	0.099	0.099	0.099
W	0.420	0.420	0.420	0.420
error	0.099	0.099	0.099	0.099
WF	0.176	0.176	0.176	0.176
error	0.059	0.059	0.059	0.059
Age uncertainties	1.000	1.000	1.000	1.000
dDR/K	0.606	0.606	0.606	0.606
dDR/dC(B, K)	0.652	0.605	0.596	0.522
dDR/dA(K)	0.539	0.500	0.493	0.431
dDR/dTh	0.018	0.018	0.018	0.018
dDR/dC(B, Th)	4.821	4.956	4.606	4.485
dDR/dA(Th)	0.160	0.165	0.153	0.149
dDR/dU	0.105	0.105	0.105	0.105
dDR/dC(B, U)	0.719	0.719	0.719	0.719
dDR/dA(U)	0.209	0.206	0.166	0.176
dDR/dW	-0.355	-0.340	-0.317	-0.295
dDR/dF	-0.355	-0.340	-0.317	-0.295
dDR/C(G, K)	0.700	0.650	0.640	0.560
dDR/C(G, Th)	5.961	6.127	5.694	5.545
dDR/dC(G, U)	1.457	1.432	1.157	1.224
dDR/dCosmic	1.000	1.000	1.000	1.000
Dage/dDe	0.644	0.659	0.678	0.701
Dage/dDR	-0.414	-0.434	-0.460	-0.491

Appendix C

Sample number Laboratory code Age estimate code	SNC01-11 X441	SNC01-12 X442	SNC01-13 X443 std	SNC01-13 X443 small
De (Gy)	1.00	1.00	4.94	5.50
uncertainty	0.19	0.19	0.46	0.32
measured	0.19	0.19	0.45	0.30
0.020	0.020	0.020	0.099	0.110
Grain size				
Min. grain size (μm)	125	125	125	125
Max grain size (μm)	180	180	180	180
External gamma-dose (mGy/a)	0.553	0.553	0.555	0.555
error	0.028	0.028	0.028	0.028
Measured concentrations				
standard fractional error	0.050	0.050	0.050	0.050
% K	0.737	0.737	0.737	0.737
error (%K)	0.037	0.037	0.037	0.037
Th (ppm)	6.670	6.670	6.670	6.670
error (ppm)	0.334	0.334	0.334	0.334
U (ppm)	1.640	1.640	1.640	1.640
error (ppm)	0.082	0.082	0.082	0.082
Cosmic dose calculations				
Depth (m)	0.600	0.600	0.530	0.530
error (m)	0.050	0.050	0.050	0.050
Average overburden density (g.cm^3)	1.900	1.900	1.900	1.900
error (g.cm^3)	0.100	0.100	0.100	0.100
Latitude (deg.), north positive	52	52	52	52
Longditude (deg.), east positive	0	0	0	0
Altitude (m above sea-level))	10	10	10	10
Cosmic dose rate (μGy/ka)	0.194	0.194	0.196	0.196
error	0.021	0.021	0.023	0.023
Moisture content				
Moisture (water / wet sediment)	0.150	0.150	0.150	0.150
error	0.050	0.050	0.050	0.050
Total dose rate (mGy/a)	**1.49**	**1.49**	**1.49**	**1.49**
error (mGy/a)	**0.07**	**0.07**	**0.07**	**0.07**
% error	**4.75**	**4.75**	**4.78**	**4.78**
AGE (a)	**672**	**672**	**3310**	**3685**
error (a)	**132**	**132**	**347**	**277**
% error	**19.69**	**19.69**	**10.48**	**7.53**
years AD/BC	1331	1331	-1307	-1682

Sample number	SNC01-11	SNC01-12	SNC01-13	SNC01-13
Laboratory code	X441	X442	X443	X443
Age estimate code	0	0	std	small
Average beta-attenuation				
standard fractional error	0.050	0.050	0.050	0.050
Natural U	0.877	0.877	0.877	0.877
error	0.044	0.044	0.044	0.044
Th-232	0.822	0.822	0.822	0.822
error	0.041	0.041	0.041	0.041
K-40	0.946	0.946	0.946	0.946
error	0.047	0.047	0.047	0.047
Dose rate conversion (mGy/a)				
standard fractional error	0.050	0.050	0.050	0.050
U (ppm)				
Beta	0.146	0.146	0.146	0.146
error	0.007	0.007	0.007	0.007
Gamma	0.000	0.000	0.000	0.000
error	0.000	0.000	0.000	0.000
Th (ppm)				
Beta	0.027	0.027	0.027	0.027
error	0.001	0.001	0.001	0.001
Gamma	0.000	0.000	0.000	0.000
error	0.000	0.000	0.000	0.000
K (%)				
Beta	0.782	0.782	0.782	0.782
error	0.039	0.039	0.039	0.039
Gamma	0.000	0.000	0.000	0.000
error	0.000	0.000	0.000	0.000
Cosmic dose				
Geomagnetic latitude	54.7	54.7	54.7	54.7
Dc (mGy/a), 55N G.lat, 0 km Alt.	0.194	0.194	0.196	0.196
error	0.021	0.021	0.023	0.023
Moisture				
F	0.420	0.420	0.420	0.420
error	0.099	0.099	0.099	0.099
W	0.420	0.420	0.420	0.420
error	0.099	0.099	0.099	0.099
WF	0.176	0.176	0.176	0.176
error	0.059	0.059	0.059	0.059
Age uncertainties	1.000	1.000	1.000	1.000
dDR/K	0.606	0.606	0.606	0.606
dDR/dC(B, K)	0.571	0.571	0.571	0.571
dDR/dA(K)	0.472	0.472	0.472	0.472
dDR/dTh	0.018	0.018	0.018	0.018
dDR/dC(B, Th)	4.491	4.491	4.491	4.491
dDR/dA(Th)	0.149	0.149	0.149	0.149
dDR/dU	0.105	0.105	0.105	0.105
dDR/dC(B, U)	0.719	0.719	0.719	0.719
dDR/dA(U)	0.196	0.196	0.196	0.196
dDR/dW	-0.319	-0.319	-0.319	-0.319
dDR/dF	-0.319	-0.319	-0.319	-0.319
dDR/C(G, K)	0.614	0.614	0.614	0.614
dDR/C(G, Th)	5.553	5.553	5.553	5.553
dDR/dC(G, U)	1.365	1.365	1.365	1.365
dDR/dCosmic	1.000	1.000	1.000	1.000
Dage/dDe	0.672	0.672	0.670	0.670
Dage/dDR	-0.451	-0.451	-2.218	-2.469

Appendix D - Problems encountered in single grain OSL measurement and analysis

Several minor problems were encountered in the measurement of the single-grain D_e distributions. When the single-grain laser attachment was first installed, on a number of occasions the XY control was erratically sent to maximum position from which it had to be wound back manually after removal of the attachment cover and either one or two fuses on the control board in the Mini-Sys II box were blown. This rare event may have been software-related as it has not occurred during running with recent control software versions. Additional cooling and improved air circulation to the rear of the Risø control box was provided to overcome regular overheating of the heater-amplifier unit.

Early single-grain measurements were made with the supplied control software using single-grain holder search parameters established during equipment installation by the manufacturers (listed in Table 2 as "standard RLAHA 1"). Other aspects of the location search routine were optimized to the individual machine during installation, and were changed from the default values. At the same time as a subsequent control software upgrade in November 2002 which allows a much greater range of operator parameter control, the single-grain holder search parameters were altered to provide a second higher resolution scan of each location hole, listed as "standard RLAHA 2" in Table 2. However, two problems were encountered. Firstly, the new software version no longer automatically attached dosing information to the data files, which had to be added laboriously at a later date during data analysis. Secondly, a subtle problem with the control software caused an occasional floating point error which stopped the run when encountered. This caused a significant loss of running time, and the requirement later to "stitch" the different parts of stopped runs together. This error was encountered at least once during most measurement runs, until around early February 2003, when the hole location search parameters were restored to "standard RLAHA 1" settings. This appeared to reduce the frequency of floating point errors occurring, and improved the machine running reliability. Close contacts with the manufacturer and software writer (Dr G Duller, Aberystwyth) were maintained, and detailed reports of the nature and timing of these errors assisted in the development of improved control software. In mid-February 2003, a further control software version (SequencePro311) was installed, which appears largely to have eliminated the floating point error (though at least one bug appears to remain) and the resulting failure of runs to be completed. In late February the hole location search parameters were restored to "standard RLAHA 2" settings, again providing a more precise location routine.

There is no evidence that any of the above-described measurement problems in any way affected the quality of the data. They simply reduced the ease and rate of single-grain sample measurement during this period (November 2002 to March 2003).

Problems encountered in data analysis

The first stage of analysis of the single grain data was performed in the versatile software package, written by G Duller, "Analyst" (version 3.04b). This provides a number of different fitting models which can be used in D_e value interpolation of the single grain SAR data. Different models are appropriate to suit different dose responses and different dose intervals, and it is necessary to examine the data to select a suitable model. For most data, it is found that the "exponential plus linear" model provides the most robust fitting method, based on a visual assessment of chi-squared. The fitting is based on the Levenberg-Markhardt method, and provides an estimate of D_e uncertainty based on a pragmatic numerical approach appropriate for OSL data, in which a relatively small number of data points are measured on each growth curve. Occasionally, the fitting routine finds a solution which can be seen to be inappropriate, often resulting from growth curves that appear to decrease at

higher doses. This is an intrinsic problem of fitting rather than a problem of this software package, and results from local minima in the searched parameter space. This is here termed "mis-fitting" (see Table 3), and such results which have fulfilled the other inclusion criteria are sometimes included by Analyst. In the present study, these results have been rejected, after visual examination of the growth curve data. Occasionally, Analyst attaches a zero value to D_e estimates and their error, or sometimes just the error. In this study, these were restored to their correct value where possible, after refitting the data in Analyst, and rejected where not possible. A third form of "mis-fitting" occasionally encountered is the setting of a D_e estimate to a very large negative value. These effects are only encountered for a very small number of grains, and are mostly limited to those that have atypical and sub-optimal characteristics, and are considered to be of little practical significance.

A further observation is that occasionally no result is provided for growth curves which appear to fulfil the criteria required for adequate fitting. In this case, as no result is available, no data are included in the D_e distribution. This effect is generally observed for sensitive grains, and may represent data in which the errors introduced by repositioning between different SAR cycles are greater than the errors imposed by measurement precision alone, which are used in the fitting. These data could be exported and fitted using a different programme, possibly with modified errors to account for repositioning errors, though this was not performed for this study.